Chapter 10
Symbol Synchronization

Marvin K. Simon

As we have seen in other chapters, the operation and performance of various receiver functions can be quite sensitive to knowledge of the timing (data transition epochs) of the received data symbols. Thus, the ability to accurately estimate this parameter and continuously update the estimate, i.e., perform symbol synchronization (sync), with little knowledge of other parameters is critical to successful operation of an autonomous receiver. Traditionally, symbol synchronization techniques have been developed assuming that the data symbols are binary, the modulation format, e.g., non-return to zero (NRZ) or Manchester data, is known a priori, and carrier synchronization is perfect. Thus, the symbol synchronization problem has been solved entirely at baseband, assuming perfect knowledge of the carrier phase and frequency.

Among the various symbol sync schemes that have been proposed in the literature, by far the most popular in terms of its application in binary communication systems is the data-transition tracking loop (DTTL) [1,2]. The scheme as originally proposed in the late 1960s is an in-phase–quadrature (I-Q) structure where the I arm produces a signal representing the polarity of a data transition (i.e., a comparison of hard (± 1) decisions on two successive symbols) and the Q arm output is a signal whose absolute value is proportional to the timing error between the received signal epoch and the receiver's estimate of it. The result of the product of the I and Q signals is an error signal that is proportional to this timing error, independent of the direction of the transition. Although originally introduced as an efficient symbol synchronization means for tracking an NRZ data signal received in additive white Gaussian noise (AWGN), it was later demonstrated (although not formally published) that the closed-loop DTTL structure can be obtained from a suitable interpretation of the maximum

a posteriori (MAP) open-loop estimate of symbol timing based on an observation of, say, N symbols at high symbol signal-to-noise ratio (SNR).

At the time of the DTTL's introduction, the binary communication systems in which the DTTL was employed were for the most part uncoded, and thus high symbol SNR was the region of primary interest. As time marched on, the design of communication systems became more and more power efficient through the application of error-correction coding, and as such a greater and greater demand was placed on the symbol synchronizer, which now had to operate in a low symbol[1] SNR region, with values based on today's coding technology perhaps as low as -8 dB. Since in this very low symbol SNR region, the DTTL scheme as originally proposed would no longer be the one motivated by MAP estimation theory, it is also likely that its tracking capability would be degraded in this region of operation. Despite this fact, the conventional DTTL appears to have continued to be used in coded communication applications.

Since autonomous receiver operation requires, in general, functioning over a wide range of SNRs, it is prudent to employ symbol-timing estimation and tracking schemes whose implementations can adapt themselves to this changing environment using the knowledge obtained from the SNR estimator. Furthermore, since as we have seen in a previous chapter, the SNR estimator itself requires knowledge of symbol timing, a means for obtaining a coarse estimate of this timing is essential.

In this chapter, we start out by considering the problem of obtaining symbol synchronization under the admittedly ideal assumption of perfect carrier synchronization. We refer to the class of schemes that results from solution of this problem as phase-coherent symbol synchronizers. In this context, we first review the MAP estimate of symbol timing based on an observation of a block of N symbols and then describe the means by which the conventional DTTL is motivated by this open-loop estimate. Next, we consider the appropriate modification of the DTTL so that it is motivated by the MAP estimate of symbol timing at low SNR; in particular, the I arm hard decisions are replaced by soft decisions whereupon, in the limiting case, the hard limiter is replaced by a linear device. As we shall show, such a loop will outperform the conventional DTTL at low SNR. We then consider the extension of the MAP-motivated closed-loop ideas to nonbinary modulations such as M-ary phase-shift keying (M-PSK) and quadrature amplitude modulation (QAM). Following this, we return to the open-loop MAP estimation of symbol sync and describe a sliding-window realization that provides sequential updates at the symbol (as opposed to the N-symbol block) rate and as such resembles the closed-loop techniques. Next, we investigate means of

[1] It is important to note here that, in a coded communication system, the symbol synchronizer precedes the decoder and thus performs its function on the *coded* symbols whose SNR is equal to the bit SNR times the code rate.

performing the symbol synchronization function in the absence of carrier phase information, i.e., so-called phase-noncoherent symbol synchronization. We show that a class of ad hoc symbol synchronizers previously proposed for solution of the phase-coherent symbol synchronization problem can be easily adapted to the noncoherent case. Finally, we propose a coarse symbol-timing estimator for use in the SNR estimation that is derived from the same statistics that are used to form the SNR estimate itself.

10.1 MAP-Motivated Closed-Loop Symbol Synchronization

Analogous to the maximum-likelihood (ML) approach taken in Chapter 9 on modulation classification, we first form the likelihood function (LF) of the received signal vector conditioned on the unknown parameters to be estimated. Specifically, for the case of M-PSK modulation with carrier phase and symbol timing as the unknown parameters, it was shown there that, after averaging over the data in a sequence of length-N symbols, the conditional-likelihood function (CLF) is given by

$$\mathrm{CLF}_M\left(\theta_c, \varepsilon\right) = C \exp\left[\sum_{n=0}^{N-1} \ln\left(\frac{2}{M} \sum_{q=0}^{M/2-1} \cosh\left[x_n\left(q; \theta_c, \varepsilon\right)\right]\right)\right] \tag{10-1}$$

where θ_c denotes the carrier phase, ε denotes the unknown fractional symbol timing, C is a constant independent of θ_c and ε, and

$$x_n\left(q; \theta_c, \varepsilon\right) \triangleq \frac{A}{\sigma^2} \mathrm{Re}\left\{\tilde{r}_n(\varepsilon) e^{-j\left(\left[2q + \left(1+(-1)^{M/2}\right)/2\right]\pi/M + \theta_c\right)}\right\} \tag{10-2}$$

with $A = \sqrt{2P}$ the signal amplitude (P is the transmitted power in the data)[2] and σ the standard deviation of the noise component (per dimension) of $\tilde{r}_n\left(\varepsilon\right)$. Also, in Eq. (10-2), the complex observables corresponding to the matched filter outputs at time instants $(n+\varepsilon)T,\ n = 0, 2, \cdots, N-1$ are given by

$$\tilde{r}_n\left(\varepsilon\right) = \frac{1}{T} \int_{(n+\varepsilon)T}^{(n+1+\varepsilon)T} \tilde{r}\left(t\right) p\left(t - nT - \varepsilon T\right) dt \tag{10-3}$$

[2] For simplicity of notation, we denote the data power by P rather than P_d since here we are not dealing with the power in the discrete carrier (if it exists) at all.

where $\tilde{r}(t)$ is the complex baseband received signal in the time interval $(n+\varepsilon)T \leq t \leq (n+1+\varepsilon)T$ and $p(t)$ is the pulse shape. Finally, the SNR at the complex output of the matched filter is given by $\gamma_s = A^2/(2\sigma^2) = E_s/N_0$, where $E_s = PT$ is the symbol energy and N_0 is the single-sided power spectral density of the additive noise.

For the purpose of finding the MAP estimate of symbol sync alone, we may assume perfect knowledge of the carrier phase, in which case, without any loss in generality, we can set $\theta_c = 0$. Under this assumption, the MAP estimate of symbol timing $\hat{\varepsilon}_{\text{MAP}}$ is given by

$$\hat{\varepsilon}_{\text{MAP}} = \underset{\hat{\varepsilon}}{\text{argmax}} \exp\left[\sum_{n=0}^{N-1} \ln\left(\frac{2}{M}\sum_{q=0}^{M/2-1} \cosh\left[x_n(q;\hat{\varepsilon})\right]\right)\right] \tag{10-4}$$

where now

$$\begin{aligned} & x_n(q;\varepsilon) \\ &= \frac{A}{\sigma^2}\,\text{Re}\left\{\tilde{r}_n(\varepsilon)\, e^{-j\left(\left[2q+\left(1+(-1)^{M/2}\right)/2\right]\pi/M\right)}\right\} \\ &= \frac{2\sqrt{P}}{N_0}\,\text{Re}\left\{e^{-j\left(\left[2q+\left(1+(-1)^{M/2}\right)/2\right]\pi/M\right)} \int_{(n+\varepsilon)T}^{(n+1+\varepsilon)T} \tilde{r}(t)\, p(t-nT-\varepsilon T)\, dt\right\} \end{aligned} \tag{10-5}$$

Note that the actual fractional symbol-timing offset ε is embedded in the received complex baseband signal $\tilde{r}(t)$, and thus the difference between $\hat{\varepsilon}_{\text{MAP}}$ and ε represents the normalized symbol-timing error.

As an alternative to Eq. (10-4), recognizing that the natural logarithm is a monotonic function of its argument, one can first take the natural logarithm of the CLF in Eq. (10-1), in which case the MAP estimate of symbol timing has the simpler form

$$\hat{\varepsilon}_{\text{MAP}} = \underset{\hat{\varepsilon}}{\text{argmax}} \left[\sum_{n=0}^{N-1} \ln\left(\frac{2}{M}\sum_{q=0}^{M/2-1} \cosh\left[x_n(q;\hat{\varepsilon})\right]\right)\right] \tag{10-6}$$

As is well-known in MAP-motivated closed-loop schemes, the argument can be made that, since the value of $\hat{\varepsilon}$ that maximizes the CLF is also the value at which the derivative of the CLF with respect to $\hat{\varepsilon}$ equates to zero, then one can use the CLF derivative itself as an error signal in a closed-loop symbol synchronization (tracking) configuration. As such, the MAP-motivated symbol synchronization loop would form

$$e = \frac{d}{d\hat{\varepsilon}} \left[\sum_{n=0}^{N-1} \ln \left(\frac{2}{M} \sum_{q=0}^{M/2-1} \cosh \left[x_n \left(q; \hat{\varepsilon} \right) \right] \right) \right]$$
$$= \sum_{n=0}^{N-1} \frac{\sum_{q=0}^{M/2-1} \sinh \left[x_n \left(q; \hat{\varepsilon} \right) \right] \frac{d}{d\hat{\varepsilon}} x_n \left(q; \hat{\varepsilon} \right)}{\sum_{q=0}^{M/2-1} \cosh \left[x_n \left(q; \hat{\varepsilon} \right) \right]} \tag{10-7}$$

as its error signal. Furthermore,

$$\begin{aligned} & x_n' \left(q; \hat{\varepsilon} \right) \\ & = \frac{A}{\sigma^2} \operatorname{Re} \left\{ \frac{d}{d\hat{\varepsilon}} \tilde{r}_n \left(\hat{\varepsilon} \right) e^{-j\left(\left[2q + \left(1 + (-1)^{M/2} \right)/2 \right] \pi / M \right)} \right\} \\ & = \frac{2\sqrt{P}}{N_0} \operatorname{Re} \left\{ e^{-j\left(\left[2q + \left(1 + (-1)^{M/2} \right)/2 \right] \pi / M \right)} \int_{(n+\hat{\varepsilon})T}^{(n+1+\hat{\varepsilon})T} \tilde{r} \left(t \right) \frac{dp \left(t - nT - \hat{\varepsilon} T \right)}{d\hat{\varepsilon}} dt \right\} \\ & = \frac{2\sqrt{P}}{N_0} \operatorname{Re} \left\{ -Te^{-j\left(\left[2q + \left(1 + (-1)^{M/2} \right)/2 \right] \pi / M \right)} \int_{(n+\hat{\varepsilon})T}^{(n+1+\hat{\varepsilon})T} \tilde{r} \left(t \right) p' \left(t - nT - \hat{\varepsilon} T \right) dt \right\} \end{aligned} \tag{10-8}$$

where the second equation follows from the Leibnitz rule, assuming $p(0) = p(T) = 0$. A closed-loop configuration that implements the expression in Eq. (10-7) as an error signal is referred to as a MAP estimation loop.

10.2 The DTTL as an Implementation of the MAP Estimation Loop for Binary NRZ Signals at High SNR

For binary signals ($M = 2$), the error signal of Eq. (10-7) simplifies to

$$e = \sum_{n=0}^{N-1} \tanh \left[x_n \left(0; \hat{\varepsilon} \right) \right] \frac{d}{d\hat{\varepsilon}} x_n \left(0; \hat{\varepsilon} \right) \tag{10-9}$$

where

$$\begin{aligned} x_n \left(0; \hat{\varepsilon} \right) &= \frac{2\sqrt{P}}{N_0} \int_{(n+\hat{\varepsilon})T}^{(n+1+\hat{\varepsilon})T} r \left(t \right) p \left(t - nT - \hat{\varepsilon} T \right) dt \\ x_n' \left(0; \hat{\varepsilon} \right) &= \frac{-2T\sqrt{P}}{N_0} \int_{(n+\hat{\varepsilon})T}^{(n+1+\hat{\varepsilon})T} r \left(t \right) p' \left(t - nT - \hat{\varepsilon} T \right) dt \end{aligned} \tag{10-10}$$

and $r(t)$ is now a real signal. A block diagram of a MAP estimation loop that uses e of Eq. (10-9) as an error signal to control a timing-pulse generator is illustrated in Fig. 10-1, where the shorthand notation $T_n(\hat{\varepsilon})$ has been introduced to represent the time interval $(n+\hat{\varepsilon})T \le t \le (n+1+\hat{\varepsilon})T$. In this figure, the accumulator represents the summation over N in Eq. (10-9). Thus, based on the above model, the loop would update itself in blocks of N symbols. In practice, however, one would replace this block-by-block accumulator by a digital filter that updates the loop every T seconds and whose impulse response is chosen to provide a desired dynamic response for the loop. The design of this filter and its associated closed-loop response characteristic are not dictated by the MAP estimation theory, which explains the use of the term "MAP-motivated" when describing the MAP estimation loop.

To go from the MAP estimation loop to the conventional DTTL, one needs to (1) approximate the hyperbolic tangent nonlinearity for large values of its argument, equivalently, at high SNR and (2) characterize, i.e., approximate, the derivative of the pulse shape required in Eq. (10-10). Specifically, for large values of its argument, one has the approximation

$$\tanh x \cong \operatorname{sgn} x \tag{10-11}$$

In theory, if $p(t)$ were a unit amplitude rectangular pulse shape, as would be the case for NRZ signals, then the derivative of $p(t)$ would be a positive delta function at the leading edge and a negative delta function at the trailing edge of the symbol interval. In practice, these unrealizable delta functions are replaced by a pair of narrow rectangular pulses whose width is treated as a design parameter. Denoting this pulse width by ξT, the above representation for two successive symbol intervals is shown in Fig. 10-2, where for simplicity of illustration we have assumed $\varepsilon = \hat{\varepsilon} = 0$. If we now group these pulses in pairs corresponding to

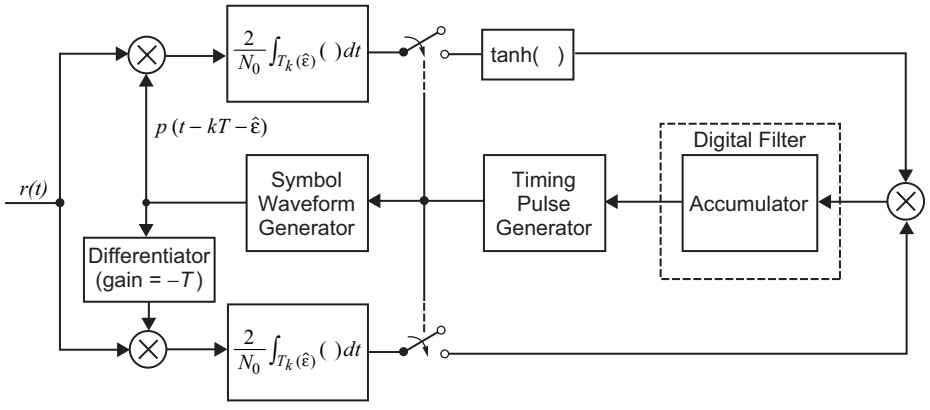

Fig. 10-1. A closed-loop symbol synchronizer motivated by the MAP estimation approach.

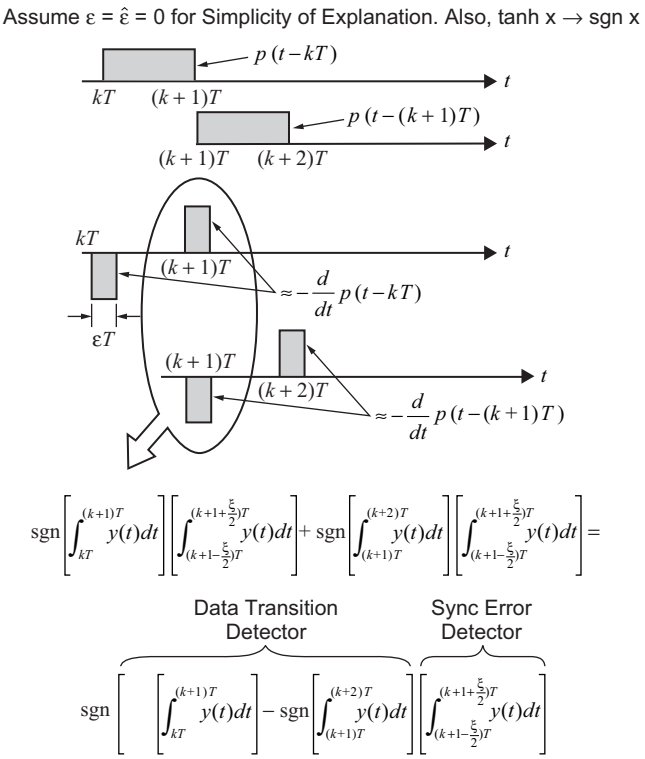

Fig. 10-2. Formation of the error signal from narrow-pulse approximation of the derivative of the pulse shape.

the trailing edge of one symbol and the leading edge of the next, then taking into account the approximation of the nonlinearity in Eq. (10-11), the contribution of the nth pair to the error signal in Eq. (10-9) would be expressed as

$$\begin{aligned} e_n = & \tanh\left(\frac{2\sqrt{P}}{N_0}\int_{nT}^{(n+1)T} r\,(t)\,p\,(t-nT)\,dt\right) \\ & \times \frac{2T\sqrt{P}}{N_0}\int_{nT}^{(n+1)T} r\,(t)\,p'\,(t-nT)\,dt \\ \cong & \left(\frac{2T\sqrt{P}}{N_0}\int_{(n+1-\xi/2)T}^{(n+1+\xi/2)T} r\,(t)\,dt\right)\left[\operatorname{sgn}\left(\frac{2\sqrt{P}}{N_0}\int_{nT}^{(n+1)T} r\,(t)\,dt\right)\right. \\ & \left.-\operatorname{sgn}\left(\frac{2\sqrt{P}}{N_0}\int_{(n+1)T}^{(n+2)T} r\,(t)\,dt\right)\right] \end{aligned} \tag{10-12}$$

The first factor in the final result of Eq. (10-12) represents an integration of width ξT *across* the data transition instant (often referred to as the window width of the synchronizer), whereas the second factor represents the difference of hard decisions on integrations *within* two successive symbol intervals. In the presence of a symbol-timing offset, when a data transition occurs, the first factor would provide a measure of the error between the actual symbol timing and the estimate of it produced by the loop. Thus, this factor is referred to as a sync error detector. The second factor is a measure of the *occurrence* of a transition in the data and thus is referred to as a data transition detector. Since the output of the sync error detector integrate-and-dump (I&D) occurs at time $(n + \xi/2)T$, where the data transition decision occurs at time $(n + 1)\,T$, one must delay the output of the former by an amount $(1 - \xi/2)T$ before the two can be multiplied. Based on the above assumptions and discussion, it is now clear that the MAP estimation loop migrates to the DTTL as illustrated in Fig. 10-3.

10.3 Conventional versus Linear Data Transition Tracking Loop

In the previous section, we observed that under high SNR conditions, where the nonlinearity is approximated as in Eq. (10-11), the I arm of the resulting symbol synchronizer becomes a detector of a transition in hard decisions made on successive symbols. In this section, we consider the synchronizer that results from approximating the nonlinearity for small values of its arguments, as would be appropriate at low SNR. It will be shown that, depending on the Q arm window width, there always exists a value of symbol SNR at which the

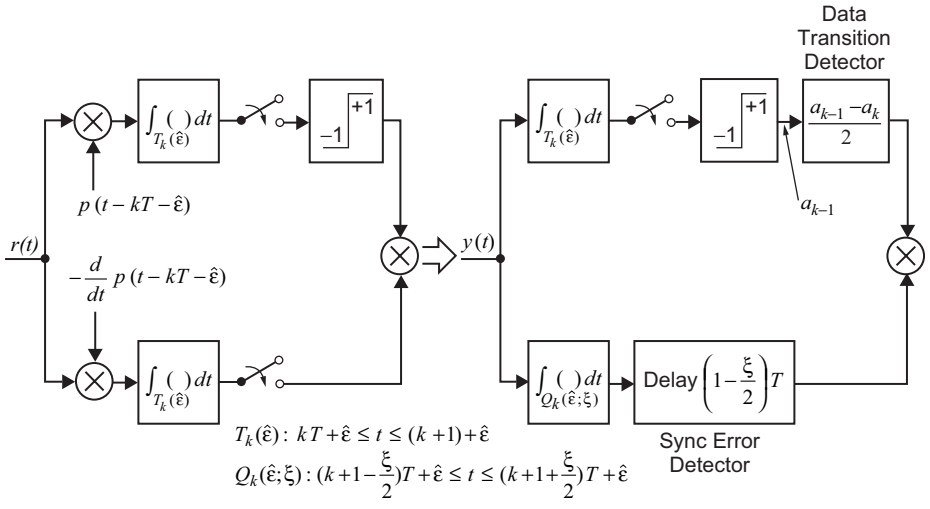

Fig. 10-3. Conventional DTTL derived from MAP estimation loop at high SNR.

linear data-transition tracking loop (LDTTL) outperforms the conventional DTTL with a hard decision I arm transition detector.

For sufficiently small values of its argument, the hyperbolic tangent nonlinearity can be approximated by

$$\tanh x \cong x \tag{10-13}$$

i.e., a linear function. Under this assumption, the appropriate MAP-motivated closed-loop synchronizer is illustrated in Fig. 10-4, and its performance is analyzed as follows. After perfect (known carrier phase) demodulation by the carrier reference $\sqrt{2}\cos(\omega_c t + \theta_c)$, the baseband signal input to the LDTTL is given by

$$\begin{aligned} r(t) &= s(t,\varepsilon) + n(t) \\ s(t,\varepsilon) &= \sqrt{P}\sum_{n=-\infty}^{\infty} d_n p(t - nT - \varepsilon T) \end{aligned} \tag{10-14}$$

where, consistent with the assumption of NRZ data, $p(t)$ is a unit amplitude rectangular pulse of duration T seconds and $\{d_n\}$ is an independent, identically distributed (iid) ± 1 sequence with d_n representing the polarity of the nth data symbol. The additive noise is a white Gaussian process with single-sided power spectral density N_0 W/Hz. The local clock produces a timing reference for the I and Q I&D filters that depends on its estimate $\hat{\varepsilon}$ of ε. Thus, the outputs of these filters corresponding to the nth symbol interval are respectively given by

$$\begin{aligned} y_{In} =& K_1 \int_{(n+\hat{\varepsilon})T}^{(n+1+\hat{\varepsilon})T} r(t)dt = \overbrace{K_1 \int_{(n+\hat{\varepsilon})T}^{(n+1+\hat{\varepsilon})T} s(t,\varepsilon)dt}^{c_n} \\ &+ \overbrace{K_1 \int_{(n+\hat{\varepsilon})T}^{(n+1+\hat{\varepsilon})T} n(t)dt}^{\nu_n} \\ y_{Qn} =& K_2 \int_{\left(n+1-\frac{\xi}{2}+\hat{\varepsilon}\right)T}^{\left(n+1+\frac{\xi}{2}+\hat{\varepsilon}\right)T} r(t)dt = \overbrace{K_2 \int_{\left(n+1-\frac{\xi}{2}+\hat{\varepsilon}\right)T}^{\left(n+1+\frac{\xi}{2}+\hat{\varepsilon}\right)T} s(t,\varepsilon)dt}^{b_n} \\ &+ \overbrace{K_2 \int_{\left(n+1-\frac{\xi}{2}+\hat{\varepsilon}\right)T}^{\left(n+1+\frac{\xi}{2}+\hat{\varepsilon}\right)T} n(t)dt}^{\mu_n} \end{aligned} \tag{10-15}$$

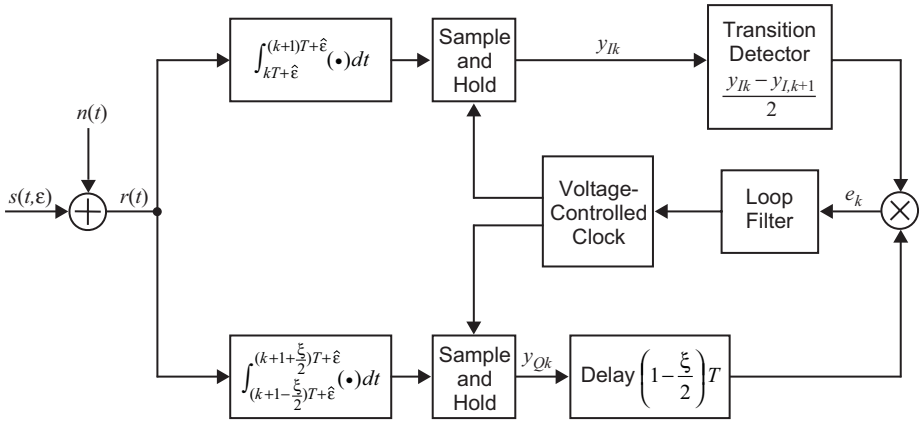

Fig. 10-4. The linear data transition tracking loop (LDTTL).

Since μ_n and ν_n are not independent, it is convenient, as was done in [1,2], to express them in terms of a new set of variables:

$$\begin{aligned}\nu_n &= N_n + M_n \\ \mu_n &= N'_{n+1} + M'_n\end{aligned} \tag{10-16}$$

where

$$\begin{aligned}N_n &= K_1 \int_{(n+\hat{\varepsilon})T}^{\left(n+\frac{1}{2}+\hat{\varepsilon}\right)T} n(t)dt, \quad M_n = K_1 \int_{\left(n+\frac{1}{2}+\hat{\varepsilon}\right)T}^{(n+1+\hat{\varepsilon})T} n(t)dt \\ N'_n &= K_2 \int_{(n+\hat{\varepsilon})T}^{\left(n+\frac{\xi}{2}+\hat{\varepsilon}\right)T} n(t)dt, \quad M'_n = K_2 \int_{\left(n+1-\frac{\xi}{2}+\hat{\varepsilon}\right)T}^{(n+1+\hat{\varepsilon})T} n(t)dt\end{aligned} \tag{10-17}$$

with the properties

N_k, M_n are mutually independent for all k, n

N'_k, M'_n are mutually independent for all k, n

N'_k, M_n and M'_k, N_n are mutually independent for all k, n

N'_k, N'_n and M_k, M_n are mutually independent for all $k \neq n$

Furthermore, all M_n, M'_n, N_n, N'_n, and their sums are Gaussian random variables with zero mean and variances

$$\sigma_{M_n}^2 = \sigma_{N_n}^2 = K_1^2 N_0 T/4$$
$$\sigma_{M_n'}^2 = \sigma_{N_n'}^2 = K_2^2 \xi N_0 T/4 \tag{10-18}$$

Taking the difference of two successive soft decisions y_{In} and $y_{I,n-1}$ and multiplying the average of the result by the quadrature I&D output (delayed by $(1-\xi/2)\,T$) gives the loop-error signal (prior to digital filtering),

$$e(t) = e_n = \left(b_n + M_n' + N_{n+1}'\right)\left[\frac{(c_n + M_n + N_n) - (c_{n+1} + M_{n+1} + N_{n+1}}{2}\right],$$
$$(n+2)T + \hat{\varepsilon} \le t \le (n+3) + T + \hat{\varepsilon} \tag{10-19}$$

which is a piecewise constant (over intervals of T seconds) random process. In Eq. (10-19),

$$b_n = \begin{cases} K_2\sqrt{P}T\left[d_n\left(\dfrac{\xi}{2}+\lambda\right) + d_{n+1}\left(\dfrac{\xi}{2}-\lambda\right)\right], & 0 \le \lambda \le \dfrac{\xi}{2} \\ K_2\sqrt{P}T d_n \xi, & \dfrac{\xi}{2} \le \lambda \le \dfrac{1}{2} \end{cases} \tag{10-20}$$
$$c_n = K_1\sqrt{P}T\left[d_{n-1}\lambda + d_n\left(1-\lambda\right)\right], \quad 0 \le \lambda \le \frac{1}{2}$$

where $\lambda \triangleq \varepsilon - \hat{\varepsilon},\ -1/2 \le \lambda \le 1/2$ denotes the normalized timing error.

10.3.1 The Loop S-Curve

The S-curve of the loop is by definition the statistical average of the error signal of Eq. (10-19) over the signal and noise probability distributions, i.e.,

$$g\left(\lambda\right) \triangleq E\left\{\left(b_n + M_n' + N_{n+1}'\right)\left[\frac{(c_n + M_n + N_n) - (c_{n+1} + M_{n+1} + N_{n+1})}{2}\right]\right\} \tag{10-21}$$

Substituting Eq. (10-20) into Eq. (10-21) and performing the necessary averaging over the noise and the data symbols d_{n-2}, d_{n-1}, and d_n gives the desired result, namely,

$$g_n(\lambda) \triangleq \frac{g(\lambda)}{K_1 K_2 P T^2} = \begin{cases} \lambda\left(1-\dfrac{\xi}{4}\right) - \dfrac{3}{2}\lambda^2, & 0 \le \lambda \le \dfrac{\xi}{2} \\ \dfrac{\xi}{2}(1-2\lambda), & \dfrac{\xi}{2} \le \lambda \le \dfrac{1}{2} \end{cases} \tag{10-22}$$

where the n subscript here stands for normalization. By comparison, the result corresponding to Eq. (10-22) for the DTTL is [1,2]

$$g_n(\lambda) \triangleq \frac{g(\lambda)}{K_2\sqrt{P}T} = \begin{cases} \lambda \operatorname{erf}\left(\sqrt{R_s}(1-2\lambda)\right) - \dfrac{1}{8}(\xi - 2\lambda) \\ \times \left[\operatorname{erf}\left(\sqrt{R_s}\right) - \operatorname{erf}\left(\sqrt{R_s}(1-2\lambda)\right)\right], & 0 \le \lambda \le \dfrac{\xi}{2} \\ \dfrac{\xi}{2}\operatorname{erf}\left(\sqrt{R_s}(1-2\lambda)\right), & \dfrac{\xi}{2} \le \lambda \le \dfrac{1}{2} \end{cases} \tag{10-23}$$

where $R_s \triangleq PT/N_0$ denotes the symbol SNR. Without belaboring the analysis, it is also straightforward to show that for $-(1/2) \le \lambda \le 0$, $g(\lambda) = -g(-\lambda)$, i.e., the S-curve is an odd function of the normalized timing error. Also note from Eq. (10-22) that the normalized S-curve for the LDTTL is independent of SNR, whereas that for the conventional DTTL [see Eq. (10-23)] is highly dependent on SNR. Figure 10-5 is an illustration of the S-curve in Eq. (10-22) for various values of window width ξ.

The slope of the normalized S-curve at the origin ($\lambda = 0$) will be of interest in computing the mean-squared timing-jitter performance. Taking the derivative of Eq. (10-22) with respect to λ and evaluating the result at $\lambda = 0$ gives for the LDTTL

$$K_g \triangleq \frac{dg(\lambda)}{d\lambda}\Big|_{\lambda=0} = K_1 K_2 P T^2 \left(1 - \frac{\xi}{4}\right) \tag{10-24}$$

whereas the corresponding result for the DTTL, based on the derivative of Eq. (10-23), is

$$K_g \triangleq \frac{dg(\lambda)}{d\lambda}\Big|_{\lambda=0} = K_2\sqrt{P}T\left[\operatorname{erf}\left(\sqrt{R_s}\right) - \frac{\xi}{2}\sqrt{\frac{R_s}{\pi}}\exp(-R_s)\right] \tag{10-25}$$

which clearly degrades with decreasing R_s.

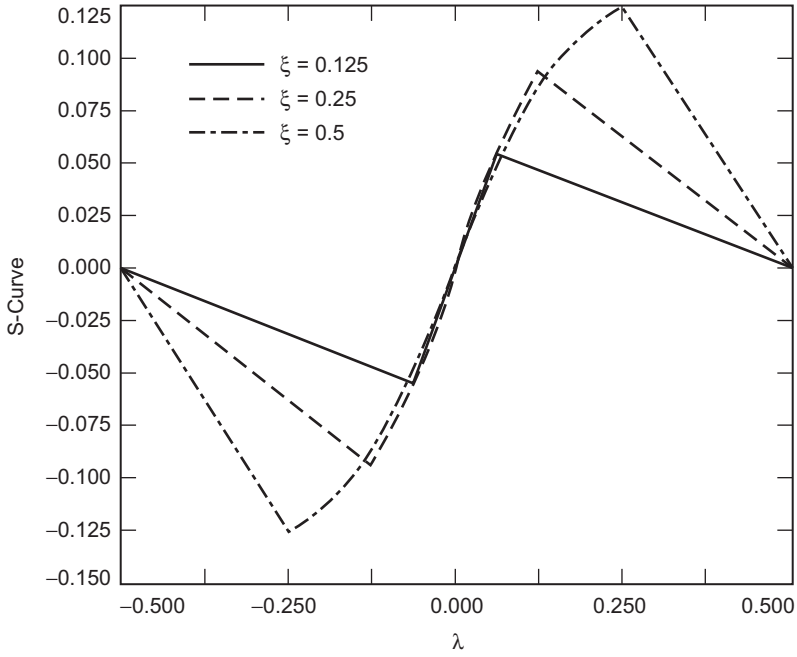

Fig. 10-5. Normalized S-curves for linear DTTL.

10.3.2 Noise Performance

The stochastic differential equation that characterizes the operation of the DTTL or the LDTTL is [1,2]

$$\dot{\lambda} = -KF(p)\left[g(\lambda) + n_\lambda(t)\right] \tag{10-26}$$

where K is the total loop gain, $F(p)$ is the transfer function of the loop filter with p denoting the Heaviside operator, and $n_\lambda(t)$ is the equivalent additive noise that characterizes the variation of the loop-error signal around its mean (the S-curve). Because of the I&D and sample-and-hold operations in the I and Q arms of the loops, $n_\lambda(t)$ is a piecewise (over intervals of T seconds) constant random process. In particular,

$$n_\lambda(t) = e_n - E\{e_n\} = e_n - g(\lambda), \quad (n+2+\hat{\varepsilon})T \le t \le (n+3+\hat{\varepsilon})T \tag{10-27}$$

with a covariance function that is piecewise linear between the sample values

$$
\begin{aligned}
R_n(\tau)\,|_{\tau=mT} &= E\{n_\lambda(t)\,n_\lambda(t+\tau)\}\,|_{\tau=mT} \\
&= E\{(e_n - E\{e_n\})\,(e_{n+m} - E\{e_{n+m}\})\} \\
&= E\{e_n e_{n+m}\} - g^2(\lambda) \triangleq R(m,\lambda), \quad m = 0, \pm 1, \pm 2, \cdots
\end{aligned} \tag{10-28}
$$

As is customary in the analysis of loops of this type, for loop bandwidths that are small compared to the reciprocal of the symbol time interval, $n_\lambda(t)$ can be approximated by a delta-correlated process with equivalent flat (with respect to frequency) power spectral density

$$
N_0' \triangleq 2\int_{-\infty}^{\infty} R_n(\tau)d\tau = 2T\left[R(0,\lambda) + 2\sum_{m=1}^{\infty} R(m,\lambda)\right] \tag{10-29}
$$

Furthermore, for large loop SNR,[3] it is customary to consider only the value of the equivalent power spectral density at $\lambda = 0$, namely,

$$
\begin{aligned}
N_0' &= 2T\left[R(0,0) + 2\sum_{m=1}^{\infty} R(m,0)\right] \\
&= 2T\left[E\left\{e_n^2\,|_{\lambda=0}\right\} + 2\sum_{m=1}^{\infty} E\{e_n e_{n+m}\,|_{\lambda=0}\}\right]
\end{aligned} \tag{10-30}
$$

With a good deal of effort, the following results can be obtained from Eq. (10-19):

$$
\begin{aligned}
&E\left\{e_n^2|_{\lambda=0}\right\} = \\
&\frac{1}{4}\Big[E\left\{b_n^2\,(c_{n+1}-c_n)^2\,|_{\lambda=0}\right\} + E\left\{b_n^2\right\} \\
&\times E\left\{(N_{n+1}+M_{n+1})^2 + (N_n+M_n)^2\right\} + E\left\{(c_{n+1}-c_n)^2\,|_{\lambda=0}\right\} \\
&\times E\left\{\left(N_{n+1}'+M_n'\right)^2\right\} + E\left\{\left(N_{n+1}'+M_n'\right)^2 (N_n+M_n-N_{n+1}-M_{n+1})^2\right\}\Big]
\end{aligned} \tag{10-31}
$$

[3] Note that this assumption does not require that the symbol SNR be large. Large loop SNR simply implies that the loop operates in the so-called linear region, i.e., where the mean-squared value of the timing error is small and the probability density function of the timing error is Gaussian distributed.

$$E\{e_n e_{n+1}|_{\lambda=0}\} = \frac{1}{4}\Big[E\{b_n b_{n+1}(c_{n+1}-c_n)(c_{n+2}-c_{n+1})|_{\lambda=0}\} - E\{b_n b_{n+1}|_{\lambda=0}\}E\left\{(N_{n+1}+M_{n+1})^2\right\}\Big] \quad (10\text{-}32)$$

$$E\{e_n e_{n+m}|_{\lambda=0}\} = 0, \quad m \neq 0,1 \quad (10\text{-}33)$$

Averaging Eqs. (10-31) through (10-33) over the signal (data sequence) and then using Eq. (10-18), we obtain the desired results, namely,

$$R(0,0) \triangleq E\left\{e_n^2|_{\lambda=0}\right\} = \left(K_1K_2PT^2\right)^2\left[\frac{\xi}{4R_s}\left(1+\frac{\xi}{2}+\frac{1}{2R_s}\right)\right] \quad (10\text{-}34)$$

$$R(1,0) \triangleq E\{e_n e_{n+1}|_{\lambda=0}\} = -\left(K_1K_2PT^2\right)^2\frac{\xi^2}{32R_s} \quad (10\text{-}35)$$

$$R(m,0) \triangleq E\{e_n e_{n+m}|_{\lambda=0}\} = 0, \quad m \neq 0,1 \quad (10\text{-}36)$$

Combining Eqs. (10-34) through (10-36), the equivalent power spectral density is then

$$N_0' = T\left(K_1K_2PT^2\right)^2\left[\frac{\xi}{2R_s}\left(1+\frac{\xi}{4}+\frac{1}{2R_s}\right)\right] \quad (10\text{-}37)$$

The equivalent quantity for the conventional DTTL can be obtained from the results in [1,2] to be

$$N_0' = T\left(K_2\sqrt{P}T\right)^2\left[\frac{\xi}{2R_s}\left[1+\frac{\xi R_s}{2}-\frac{\xi}{2}\left[\frac{1}{\sqrt{\pi}}\exp(-R_s)+\sqrt{R_s}\,\mathrm{erf}\sqrt{R_s}\right]^2\right]\right] \quad (10\text{-}38)$$

10.3.3 Mean-Squared Timing-Error Performance

The mean-squared timing jitter σ_λ^2 of either the LDTTL or the DTTL is readily computed for a first-order loop filter ($F(p) = 1$) and large loop SNR conditions. In particular, linearizing the S-curve to $g(\lambda) = K_g\lambda$ and denoting the single-sided loop bandwidth by B_L, we obtain

$$\sigma_\lambda^2 = \frac{N_0' B_L}{K_g^2} \tag{10-39}$$

where K_g is obtained from either Eq. (10-24) or Eq. (10-25) and N_0' from either Eq. (10-37) or Eq. (10-38). Making the appropriate substitutions in Eq. (10-39) gives the results

$$\sigma_\lambda^2 = \frac{\xi\left[1 + \frac{\xi}{4} + \frac{1}{2R_s}\right]}{2\rho\left(1 - \frac{\xi}{4}\right)^2} \text{ (LDTTL)}$$

$$\sigma_\lambda^2 = \frac{\xi\left[1 + \frac{\xi R_s}{2} - \frac{\xi}{2}\left[\frac{1}{\sqrt{\pi}}\exp\left(-R_s\right) + \sqrt{R_s}\,\text{erf}\,\sqrt{R_s}\right]^2\right]}{2\rho\left[\text{erf}\left(\sqrt{R_s}\right) - \frac{\xi}{2}\sqrt{\frac{R_s}{\pi}}\exp\left(-R_s\right)\right]^2} \text{ (DTTL)} \tag{10-40}$$

where $\rho \triangleq P/N_0 B_L$ is the so-called phase-locked loop SNR. Figure 10-6 is a plot of the ratio of $\sigma_\lambda^2\big|_{\text{LDTTL}}$ to $\sigma_\lambda^2\big|_{\text{DTTL}}$ in dB as a function of R_s in dB

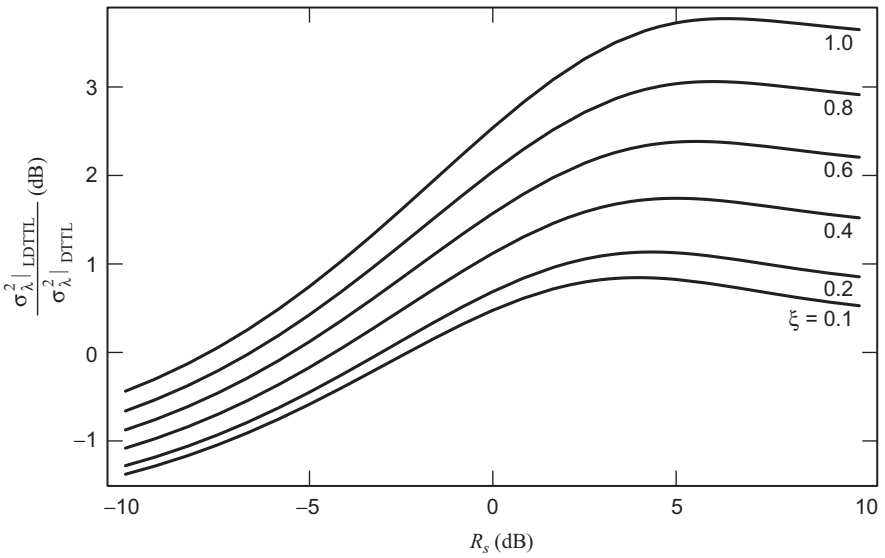

Fig. 10-6. Mean-squared jitter comparison of the nonlinear and linear DTTLs.

with quadrature arm normalized window width ξ as a parameter. The numerical results clearly illustrate the performance advantage of the LDTTL at low symbol SNRs. In fact, in the limit of sufficiently small SNR, the ratio of the variances approaches the limit

$$\lim_{R_s \to 0} \frac{\sigma_\lambda^2 \,|\, \text{LDTTL}}{\sigma_\lambda^2 \,|\, \text{DTTL}} = \frac{\left(2 - \frac{\xi}{2}\right)^2}{2\pi \left(1 - \frac{\xi}{4}\right)^2 \left(1 - \frac{\xi}{2\pi}\right)} \tag{10-41}$$

which for $\xi = 0$ (the theoretical value suggested by the MAP estimation of symbol sync approach) becomes

$$\lim_{\substack{R_s \to 0 \\ \xi \to 0}} \frac{\sigma_\lambda^2 \,|\, \text{LDTTL}}{\sigma_\lambda^2 \,|\, \text{DTTL}} = \frac{2}{\pi} \tag{10-42}$$

The fact that this ratio approaches a finite limit is not surprising in view of a similar behavior for other synchronization loops motivated by the MAP estimation approach. For example, when comparing the conventional Costas loop (motivated by the low SNR approximation to the MAP estimation of carrier phase) to the polarity-type Costas loop (motivated by the high SNR approximation to the MAP estimation of carrier phase), the ratio of variances of the phase error is given by (see Chapter 8)

$$\frac{\sigma_\phi^2 \,|_{\text{Conventional}}}{\sigma_\phi^2 \,|_{\text{Polarity-Type}}} = \frac{\text{erf}^2\left(\sqrt{R_s}\right)}{2R_s/\left(1 + 2R_s\right)} \tag{10-43}$$

which for sufficiently small SNR becomes

$$\lim_{R_s \to 0} \frac{\sigma_\phi^2 \,|_{\text{Conventional}}}{\sigma_\phi^2 \,|_{\text{Polarity-Type}}} = \frac{2}{\pi} \tag{10-44}$$

For large symbol SNR, the ratio of the variances in Eq. (10-40) approaches

$$\lim_{R_s \to \infty} \frac{\sigma_\lambda^2 \,|\, \text{LDTTL}}{\sigma_\lambda^2 \,|\, \text{DTTL}} = \frac{1 + \frac{\xi}{4}}{\left(1 - \frac{\xi}{4}\right)^2} \tag{10-45}$$

which for small window widths results in a small penalty for removing the I arm hard limiter.

10.4 Simplified MAP-Motivated Closed-Loop Symbol Synchronizers for *M*-PSK

In Section 10.1, we derived the form of the error signal [see Eq. (10-7)] for a MAP-motivated closed-loop symbol synchronizer of M-PSK, which is somewhat complicated at best. Applying a large argument (high SNR) approximation to the nonlinearities in the numerator and denominator of the expression in Eq. (10-7), namely, $\sinh x \cong (e^x/2)\operatorname{sgn} x$, $\cosh x \cong e^x/2$, unfortunately does not simplify matters because of the summation over the index (q) resulting from averaging over the signal constellation. In problems of this nature, it is common to approximate the summation by its largest term. In this particular case, it is most convenient to make this approximation in the CLF of Eq. (10-1) prior to taking its derivative to form the error signal in the MAP estimation loop. When this is done, we obtain for the MAP estimate (again setting $\theta_c = 0$)

$$\hat{\varepsilon}_{\mathrm{MAP}} \cong \underset{\hat{\varepsilon}}{\operatorname{argmax}} \left[\sum_{n=0}^{N-1} \ln \left(\frac{2}{M} \max_{q} \left\{ \cosh \left[x_n \left(q; \hat{\varepsilon} \right) \right] \right\} \right) \right] \tag{10-46}$$

or, equivalently, because of the monotonicity of the hyperbolic cosine function,

$$\hat{\varepsilon}_{\mathrm{MAP}} \cong \underset{\hat{\varepsilon}}{\operatorname{argmax}} \left[\sum_{n=0}^{N-1} \ln \left(\frac{2}{M} \cosh x_n \left(q_{\max}; \hat{\varepsilon} \right) \right) \right] \tag{10-47}$$

where

$$q_{\max} \triangleq \max_{q} \left\{ \left| x_n \left(q; \hat{\varepsilon} \right) \right| \right\} \tag{10-48}$$

Now differentiating Eq. (10-47) with respect to $\hat{\varepsilon}$, we obtain an expression for the error signal in a MAP-motivated symbol synchronizer for M-PSK at high SNR, namely,

$$e = \frac{d}{d\hat{\varepsilon}} \left[\sum_{n=0}^{N-1} \ln \left(\frac{2}{M} \cosh x_n \left(q_{\max}; \hat{\varepsilon} \right) \right) \right] = \sum_{n=0}^{N-1} \tanh \left[x_n \left(q_{\max}; \hat{\varepsilon} \right) \right] \frac{d}{d\hat{\varepsilon}} x_n \left(q_{\max}; \hat{\varepsilon} \right) \tag{10-49}$$

Note the similarity of Eq. (10-49) to Eq. (10-9). In fact, for binary phase-shift keying (BPSK), the only value of q in the sum is $q = 0$, and thus for this case $q_{\max} = 0$, which establishes the equivalence between Eq. (10-49) and Eq. (10-9). Because of this similarity, one can immediately apply the same small and large argument approximations to the hyperbolic tangent nonlinearity and, analogous to Figs. 10-3 and 10-4, arrive at DTTL-like implementations that are illustrated in Figs. 10-7 and 10-8.

10.5 MAP Sliding-Window Estimation of Symbol Timing

As discussed in Section 10.1, open-loop MAP estimation of the symbol epoch involves finding the conditional (on the symbol timing) likelihood function of the received signal based on a single observation of the received signal over a block of symbols. Furthermore, since the unknown symbol epoch is assumed to be uniformly distributed over the symbol interval, the MAP estimate is equivalent to the ML estimate. We have also seen that the traditional closed-loop estimation scheme motivated by the MAP estimation approach employs an error signal derived from the derivative of the CLF that can be updated at intervals corresponding to the symbol time. Since for rectangular pulses, e.g., an NRZ data stream, the derivative of the CLF, which is related to the derivative of the pulse shape, is undefined, closed-loop structures motivated by the MAP estimation approach strictly speaking do not exist. Nevertheless, with suitable approximations of the derivative of the pulse shape, such a closed loop, e.g., the DTTL, will in fact provide symbol sync for an NRZ data stream with rectangular pulses; however, it does so with a degradation in performance relative to that which can be provided by the MAP or minimum mean-squared (MMS) open-loop estimators. On the other hand, the closed-loop approach provides a continuous updating (tracking) of the symbol timing (once per bit interval) that is desirable in the presence of channel dynamics, whereas the open approach usually is regarded as either a one-shot estimator, i.e., compute the MAP or MMS estimate based on a single observed long block of data, or a block-by-block estimator where the single shot is sequentially repeated over and over.

What is important to observe is that the open-loop estimation techniques can be modified to provide sequential updates at the symbol rate to the symbol-timing epoch estimates and as such resemble the closed-loop techniques with, however, improved performance. It is this issue that we wish to discuss here, namely, a simple sequential digital implementation of the MAP estimation of symbol epoch that can track the dynamics in this parameter yet provide a performance approaching that of the true optimum MAP estimation technique.

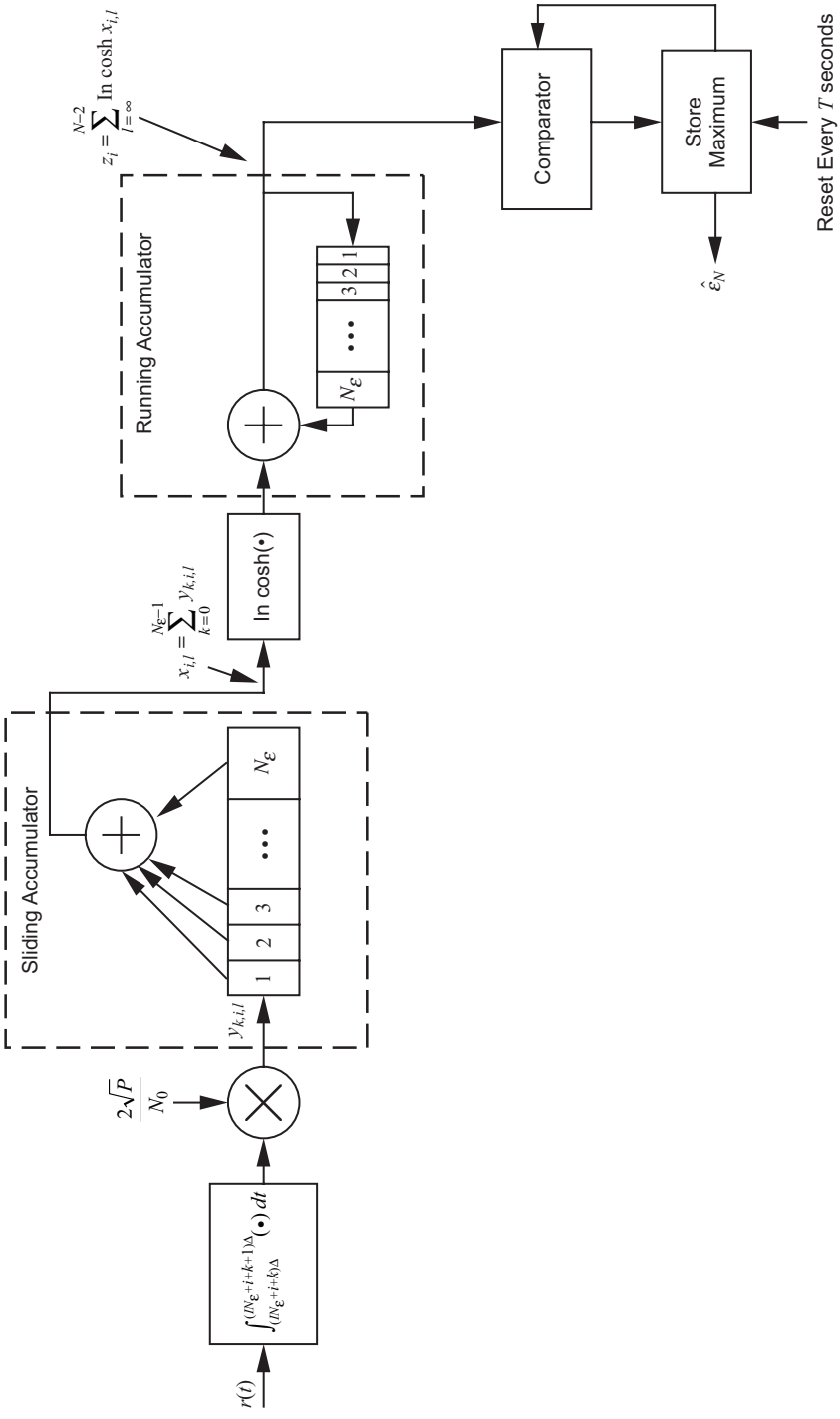

Fig. 10-7. A maximum-likelihood sliding-window estimator of timing for an NRZ data stream.

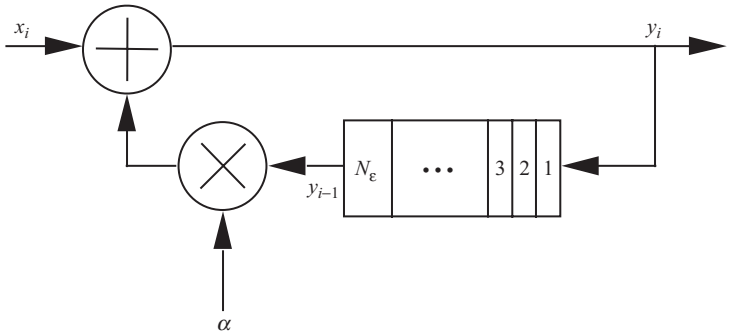

Fig. 10-8. A weighted running accumulator.

10.5.1 A Brief Discussion of Performance and Its Bounds for Open- and Closed-Loop Symbol-Timing Techniques

As we have noted in other chapters, an appropriate measure of the performance of an unbiased estimator of a parameter is its variance, which is equal to the mean-squared value of the error between the estimator and the parameter. Although it is usually difficult to arrive at an analytical expression for the variance of the MAP or MMS estimator, there exist many lower bounds on this quantity that can be evaluated analytically. The most popular of these bounds is the Cramer–Rao (C-R) bound [3–5] since it can be obtained directly from the conditional probability density function (pdf) of the received signal given the unknown epoch, which as shown earlier has the analytically desirable Gaussian form. In particular, the C-R bound on the variance of any unbiased estimator $\hat{\varepsilon}$ of ε is given by

$$\sigma_\varepsilon^2 \geq \left[E\left\{ \left(\frac{\partial \ln p\big(r(t)\,|\varepsilon\big)}{\partial \varepsilon} \right)^2 \right\} \right]^{-1} = -\left[E\left\{ \frac{\partial^2 \ln p\big(r(t)\,|\varepsilon\big)}{\partial \varepsilon^2} \right\} \right]^{-1} \triangleq \sigma_{C-R}^2 \tag{10-50}$$

In order to evaluate the derivative required in Eq. (10-50), it is necessary that the pulse shape be differentiable—the same condition as needed to form the MAP estimation loop. If the pulse shape is in fact differentiable and the other conditions for the C-R bound to exist [3–5] are satisfied, then for large SNR γ, the C-R bound varies inversely as the SNR, i.e., $\sigma_{C-R}^2 = C\gamma^{-1}$, where the constant of proportionality, C, depends on the particular pulse shape and its second derivative [5]. It is also true that, if the C-R bound is achievable, then clearly the MMS

estimator will be the one that achieves it, but so does the MAP estimator. That is, in this situation the MAP estimator is asymptotically (large SNR) efficient. On the other hand, if the C-R bound is not achievable, then by definition the more complex MMS estimator still will achieve the smallest estimator variance, and the MAP estimator may in fact result in a larger variance. That is, in this situation one cannot guarantee how close the MAP estimator comes to the C-R bound.

It can similarly be shown that closed loops motivated by the MAP approach, i.e., those that employ an error signal derived from the derivative of the LF, have a mean-squared timing error that varies inversely linearly with SNR. In the closed-loop case, one must make an appropriate adjustment to the term "SNR" to reflect the relation between the reciprocal of the loop bandwidth and the observation time of the open-loop estimate, analogously to what was done for the carrier synchronization case in Chapter 8. In particular, if the two-sided loop bandwidth is defined as equal to the reciprocal of the observation time (which is appropriate for a noise bandwidth definition), then the mean-squared timing error of the closed loop satisfies the C-R bound, i.e., $\sigma_\varepsilon^2 = \gamma^{-1}$.

When the pulse is not differentiable, such as the rectangular pulse that is characteristic of NRZ modulation, then as previously mentioned the C-R bound does not exist. One might consider trying to use the C-R bound in such situations by approximating the square pulse with a trapezoidal shape (which leads to derivatives at the edges that are rectangular pulses, as discussed in Section 10.2 for the DTTL), and then taking the limit as the slope of the edges approaches infinity. Unfortunately, when this is done the C-R bound becomes directly proportional to the inverse of the slope, and thus in the limit as the slope approaches infinity for any finite SNR, the bound degenerates to being useless, i.e., $\sigma_{C-R}^2 \to 0$.

To get around this enigma, researchers have investigated other bounds on the estimator variance that exist even when the pulse is non-differentiable. A variety of these bounds [6–9] are reviewed and compared in [10]. All of the results obtained in these references are for the case of a transmitted signal corresponding to either a single pulse, a periodic repetition of a single pulse, or a known sequence of pulses, such as a pseudo-noise (PN) code, and as such correspond to navigation, radar, and direct sequence spread spectrum system applications. For the case of data communication, where the transmitted waveform is a sequence of pulses with random (unknown) polarity, in order to make the results given in the above references applicable in this situation, one must draw an appropriate equivalence between the two scenarios. It is relatively straightforward to show that the C-R bound (which again does not apply in the square-pulse case) on the variance of the delay estimator for a random pulse stream of N symbols is equivalent to the C-R bound on the variance of a single pulse of N times the energy. Although establishing this equivalence is more formidable for the other bounds that do apply to the square-pulse case, we anticipate that a similar be-

havior will occur. Proceeding with this intuitive assumption, we now discuss the behavior of the various bounds considered in [10] as they would apply to the NRZ communication problem.

What is interesting about all the bounds in [6–9] is that, for rectangular pulses, they all predict (for large SNR) an inverse square-law behavior with SNR, i.e., $\sigma^2 \geq C\gamma^{-2}$, as opposed to the inverse linear behavior one might expect (at least from C-R bound considerations which granted do not apply here). The difference between the various bounds is the constant of proportionality, C. Monte Carlo simulations performed in [10] show that, in this situation, the MAP and MMS estimators have a similar inverse square-law behavior with SNR and come quite close to the tightest of the lower bounds. Thus, since the closed-loop schemes derived from the above-mentioned approximations to the MAP approach can achieve only inverse linear behavior with SNR, it behooves one to reexamine the possibility of using open-loop epoch estimation with the hope of obtaining a simple sequential structure that will allow for an improvement in performance as well as the ability to track variations in the parameter.

10.5.2 Formulation of the Sliding-Window Estimator

To arrive at the sliding-window version of the MAP estimator, we slightly modify the approach taken in Section 10.2 by assuming now that the observation of the received signal extends over the entire past up to the present time $t = NT$, and furthermore that the unknown parameter, ε, is constant over this observation, i.e., in the interval $-\infty \leq t \leq NT$.[4] In this case, the estimate at time NT becomes

$$\hat{\varepsilon}_N = \underset{\hat{\varepsilon}}{\operatorname{argmax}} \, \Lambda\left(\hat{\varepsilon}; NT\right) \tag{10-51}$$

where

$$\Lambda\left(\varepsilon; NT\right) \triangleq \sum_{l=-\infty}^{N-1} \ln \cosh \left(\frac{2\sqrt{P}}{N_0} \int_{-\infty}^{NT} r(t) p\left(t - lT - \varepsilon T\right) dt \right) \tag{10-52}$$

Ignoring the partial (less than a full symbol interval) contribution of the $N-1$st pulse $p\left(t - (N-1)T - \varepsilon T\right)$ [since the full contribution will be picked up in the LF for the next interval, namely, $\Lambda\left(\varepsilon; (N+1)T\right)$], we can rewrite Eq. (10-52) as

[4] Shortly we shall say more about how to tailor the results to the more practical case where the parameter is dynamic but slowly (with respect to the symbol duration) varying.

$$\Lambda\left(\varepsilon; NT\right) \triangleq \sum_{l=-\infty}^{N-2} \ln\cosh\left(\frac{2\sqrt{P}}{N_0}\int_{lT+\varepsilon}^{(l+1)T+\varepsilon} r(t)dt\right) \tag{10-53}$$

The LF as defined in Eq. (10-53) is a function of a parameter ε that takes on a continuum of values in the interval $0 \le t \le T$. In order to construct a practical implementation of Eq. (10-53), it is customary to quantize the uncertainty interval, i.e., approximate the continuous variable εT by a discrete variable that takes on values $\varepsilon_i T = iT/N_\varepsilon \triangleq i\Delta,\ i = 0, 1, 2, \cdots, N_\varepsilon - 1$. Since the quantization increment Δ determines the resolution to which the parameter can be estimated, the value of N_ε is chosen to satisfy this requirement. The time-quantized LF can now be written as

$$\Lambda\left(\varepsilon_i; NT\right) \triangleq \sum_{l=-\infty}^{N-2} \ln\cosh\left(\frac{2\sqrt{P}}{N_0}\int_{(lN_\varepsilon+i)\Delta}^{((l+1)N_\varepsilon+i)\Delta} r(t)dt\right),$$

$$i = 0, 1, 2, \cdots, N_\varepsilon - 1 \tag{10-54}$$

The integral in Eq. (10-54), which represents the integration of the received signal over the lth symbol interval (shifted by the epoch $\varepsilon_i T = i\Delta$), can be expressed as a sum of N_ε integrals over each quantization interval. In particular,

$$\Lambda\left(\varepsilon_i; NT\right) \triangleq \sum_{l=-\infty}^{N-2} \ln\cosh\left(\frac{2\sqrt{P}}{N_0}\sum_{k=0}^{N_\varepsilon-1}\int_{(lN_\varepsilon+i+k)\Delta}^{(lN_\varepsilon+i+k+1)\Delta} r(t)dt\right),$$

$$i = 0, 1, 2, \cdots, N_\varepsilon - 1 \tag{10-55}$$

Thus, the quantized MAP estimator of εT at time $t = NT$ is given by

$$\hat{\varepsilon}_N T = \hat{i}_N \Delta = \left[\underset{i}{\operatorname{argmax}}\, \Lambda\left(\hat{\varepsilon}_i; NT\right)\right]\Delta \tag{10-56}$$

The MAP estimate of symbol epoch at time $t = (N+1)\,T$ (i.e., one symbol time later) is given by

$$\hat{\varepsilon}_{N+1} T = \left[\underset{i}{\operatorname{argmax}}\, \Lambda\big(\hat{\varepsilon}_i; (N+1)\,T\big)\right]\Delta \tag{10-57}$$

where

$$\Lambda\left(\varepsilon_i;(N+1)\,T\right)=\sum_{l=-\infty}^{N-1}\ln\cosh\left(\frac{2\sqrt{P}}{N_0}\sum_{k=0}^{N_\varepsilon-1}\int_{(lN_\varepsilon+i+k)\Delta}^{(lN_\varepsilon+i+k+1)\Delta}r(t)dt\right)$$

$$=\Lambda\left(\varepsilon_i;NT\right)+\ln\cosh\left(\frac{2\sqrt{P}}{N_0}\sum_{k=0}^{N_\varepsilon-1}\int_{[(N-1)N_\varepsilon+i+k]\Delta}^{[(N-1)N_\varepsilon+i+k+1]\Delta}r(t)dt\right)\tag{10-58}$$

Thus, every T seconds (as in a closed-loop symbol synchronizer that updates its error signal every symbol time, e.g., the DTTL), we obtain an epoch estimate. An implementation of Eq. (10-56) that does not require a parallel bank of N_ε correlators as is traditional for an N_ε-quantized MAP parameter estimator is illustrated in Fig. 10-7. First, $\int_{(lN_\varepsilon+i+k)\Delta}^{(lN_\varepsilon+i+k+1)\Delta}r(t)dt$ is computed, which represents the integral of the received signal in the kth quantization (sample) interval of the lth symbol corresponding to the ith epoch position. Next, N_ε successive integrals, each scaled by $2\sqrt{P}/N_0$, are summed for each epoch position that, because of the recursive nature of the index i in Eq. (10-55), can be implemented by a sliding accumulator. That is, N_ε successive outputs of the sliding accumulator represent the argument of the "ln cosh" function in Eq. (10-55) for the N_ε epoch positions corresponding to the lth symbol. Next, we take the hyperbolic cosine of these outputs and pass them to a running accumulator (with delay equal to a symbol time or equivalently N_ε sample times.) Thus, in accordance with Eq. (10-58) each output of the running accumulator (which occurs every Δ seconds) is an accumulation of inputs spaced N_ε samples ($N\Delta=T$ seconds) apart. The output of this running accumulator in N_ε successive sampling intervals then is the quantized LF of Eq. (10-58) for the current symbol interval, namely, the Nth. The "comparator" and "store maximum" blocks then proceed to find the maximum of these N_ε likelihood values for the Nth symbol interval, after which the estimate is output. The "store maximum" block then is reset, and the procedure is repeated for the next (i.e., the N+1st) symbol interval. It is important that the "store maximum" block be reset in each symbol interval so that an erroneous symbol epoch in one symbol interval does not propagate to succeeding intervals, that is, the symbol epoch estimate for each symbol interval should be made from the maximum of the set of N_ε LF samples for that interval and not by comparison with the maximum of samples from any previous interval.

Because of the assumption that the unknown parameter being estimated, i.e., symbol epoch, is constant over the observation, the implementation in Fig. 10-7 includes a running accumulator with uniform weighting. In the more practical

case, where the parameter is dynamic but slowly varying, one can only assume that the unknown parameter is constant over a finite number of symbol intervals. As such, the uniform running accumulator should be replaced with a weighted running accumulator that reflects a fading memory and is analogous to what is done in a closed-loop architecture by using a digital filter following the error signal. The simplest method for accomplishing this is illustrated in Fig. 10-8, where the feedback term is multiplied by a constant $\alpha < 1$. This achieves a running accumulator with a geometric weighting that has the input–output characteristic

$$y_i = \sum_{m=0}^{\infty} \alpha^m x_{i-m} \tag{10-59}$$

Finally, since the running accumulator also accomplishes the data detection (matched-filter) function, then the epoch estimate index, $\hat{i}_N$, of Eq. (10-56) can be used to determine in each symbol interval which running accumulator output to use for making a hard decision on that symbol.

10.5.3 Extension to Other Pulse Shapes

When the pulse shape is other than rectangular, then, strictly speaking, the simplification that allows the bank of N_ε correlators to be replaced by a sliding accumulator as in Fig. 10-7 is not possible. However, if N_ε is large and the pulse shape is approximated by a piecewise constant staircase function with N_ε steps, then the correlation of the received signal and the pulse shape in a quantization interval can be written as

$$\int_{i\Delta}^{(i+1)\Delta} r(t)p(t)dt = p_i \int_{i\Delta}^{(i+1)\Delta} r(t)dt \tag{10-60}$$

where p_i is the assumed constant value of $p\,(t)$ in the interval $i\Delta \le t \le (i+1)\,\Delta$. In view of Eq. (10-60), the only modification of Fig. 10-7 that is necessary to allow for the inclusion of an arbitrary pulse shape is to replace the uniform sliding accumulator with a *weighted* sliding accumulator (see Fig. 10-9), where the weights are equal to the piecewise constant values of $p(t)$. Furthermore, for sufficiently large N_ε, one can approximately replace the integral of $r(t)$ over the quantization interval by the value of $r(t)$ at the midpoint of this interval times the duration of this interval, Δ. As such, the integrator at the input of Fig. 10-7 can be replaced simply by a uniform sampler at rate $1/\Delta$.

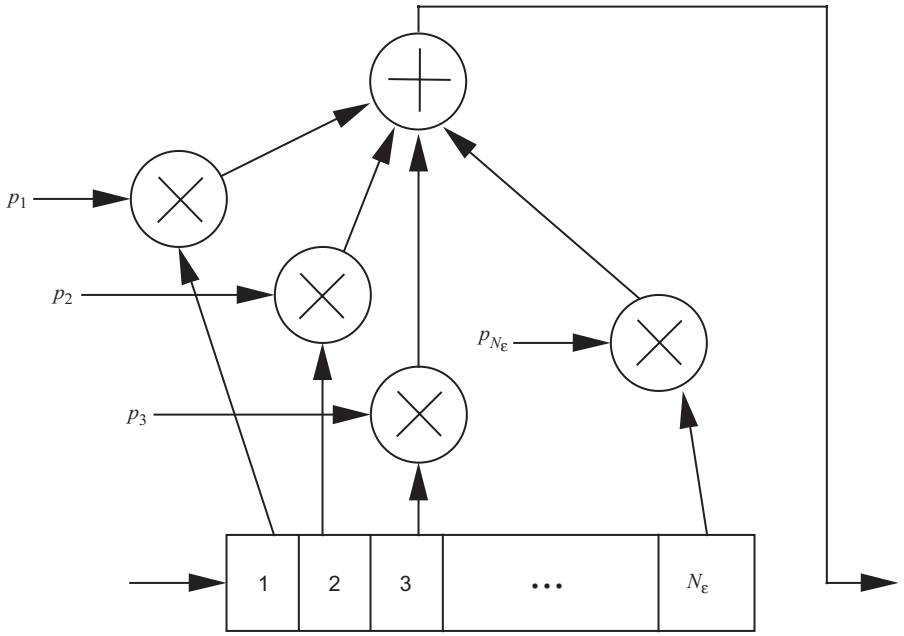

Fig. 10-9. A weighted sliding-window accumulator.

10.6 Symbol Synchronization in the Absence of Carrier Phase Information

10.6.1 Suboptimum Schemes

In addition to "optimum" symbol synchronizers, such as the ones discussed thus far that are motivated by the MAP estimation approach, several other suboptimum schemes have been proposed in the literature that offer the advantage of a simpler implementation and at the same time perform nearly as well as the more complex optimum ones. One of the more popular of these ad hoc schemes that draws its roots from the squaring loop used for carrier synchronization is called the "filter and square symbol synchronizer," whose tracking performance was analyzed in [11] for the case of an NRZ input and a single-pole Butterworth low-pass filter for $H(s)$. A block diagram of this synchronizer is provided in Fig. 10-10. The operation of this scheme is briefly summarized as follows.

For a binary NRZ input described by $s(t,\varepsilon)=\sqrt{P}\sum_{n=-\infty}^{\infty} d_n p(t-nT-\varepsilon T)$, the output of the filter is given as $\hat{s}(t,\varepsilon) = \sqrt{P}\sum_{n=-\infty}^{\infty} d_n \hat{p}(t-nT-\varepsilon T)$, where[5]

[5] Here, the hat on $s(t,\varepsilon)$ and $p(t)$ is simply used to denote the result of low-pass filtering by $H(s)$.

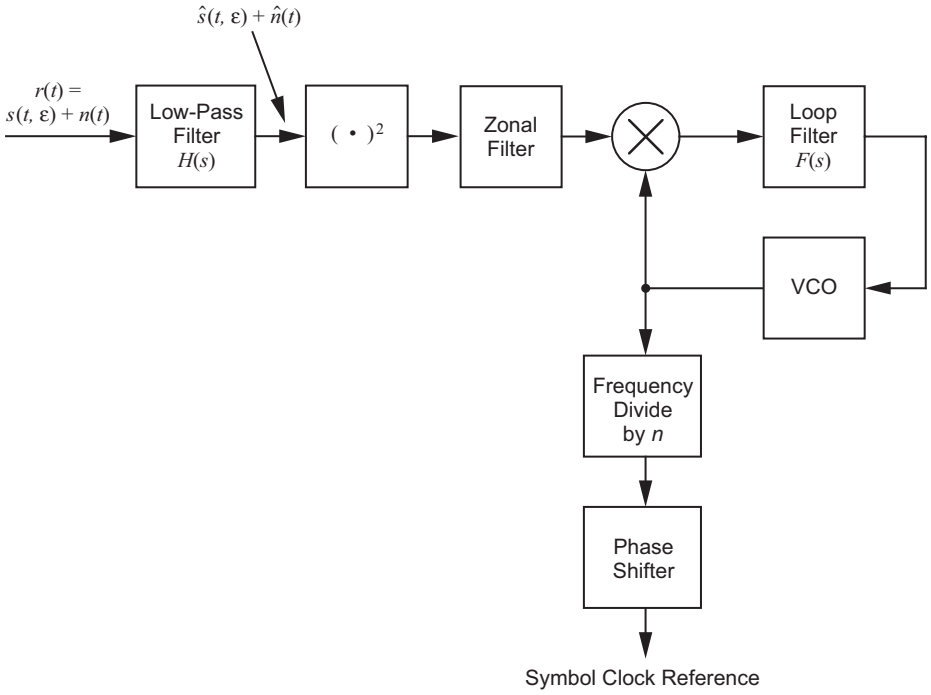

Fig. 10-10. Filter and square symbol synchronizer.

$$\hat{p}(t) = \frac{1}{2\pi} \int_{-\infty}^{\infty} P(\omega) H(\omega) d\omega \tag{10-61}$$

with $P(\omega)$ the Fourier transform of the NRZ rectangular pulse $p(t)$. Squaring $\bar{s}(t, \varepsilon)$ results in

$$\hat{s}^2(t, \varepsilon) = P \sum_{n=-\infty}^{\infty} \hat{p}^2(t - nT - \varepsilon T) + P \sum_{m=-\infty}^{\infty} \sum_{n=-\infty}^{\infty} d_m d_n \hat{p}(t - mT - \varepsilon T) \hat{p}(t - nT - \varepsilon T) \tag{10-62}$$

which after ensemble averaging over the random data becomes

$$\overline{\hat{s}^2(t, \varepsilon)} = P \sum_{n=-\infty}^{\infty} \hat{p}^2(t - nT - \varepsilon T) \tag{10-63}$$

The term $\sum_{n=-\infty}^{\infty} \hat{p}^2 (t - nT - \varepsilon T)$ is periodic with fundamental period equal to T and thus possesses a line spectrum with harmonics that are multiples of the data rate, each of which carries along the symbol-timing information. Thus, following this signal with a zonal filter (to extract, say, the nth harmonic), a sinusoidal tone is generated at $f = n/T$ that can be tracked by a phase-locked loop (PLL) whose voltage-controlled oscillator (VCO) output after frequency division by n and an appropriate phase shift[6] represents a symbol-timing clock that is synchronous with the input data stream.

Shortly thereafter [12], a generalization of the filter and square symbol synchronizer was proposed in which the square-law device was replaced by a delay-and-multiply operation (see Fig. 10-11). The resulting configuration, referred to as a "cross-spectrum symbol synchronizer (CSSS)," allowed in general for a delay element equal to a fraction α of the symbol time, where the value of α would be chosen to optimize the tracking performance in the sense of minimizing the mean-squared timing error. It is clear from a comparison of Figs. 10-10 and 10-11 that the filter and square-law symbol synchronizer is a special case of the cross-spectrum symbol synchronizer corresponding to $\alpha = 0$. Once again assuming a

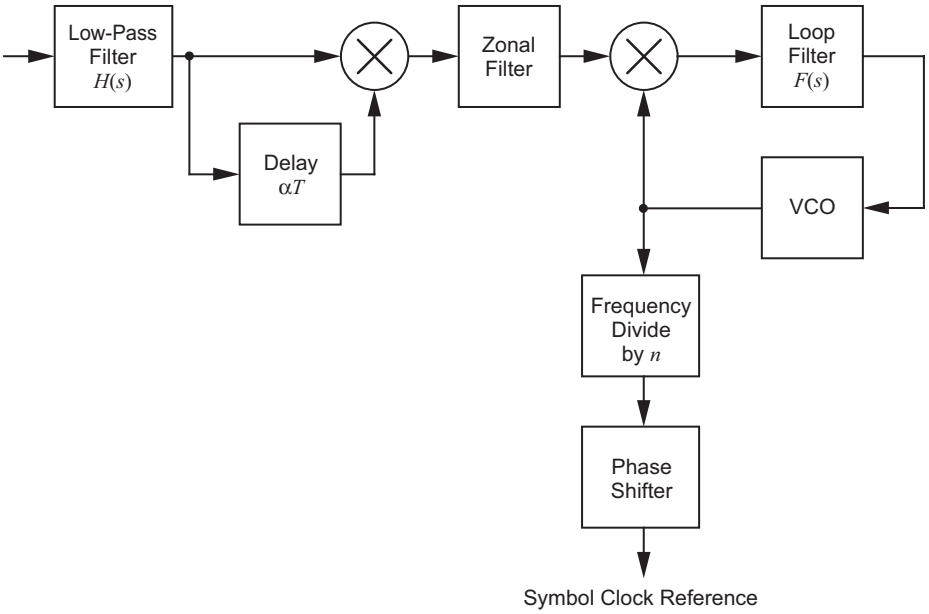

Fig. 10-11. Cross-spectrum symbol synchronizer.

[6] The phase shifter is required to cancel the known phase shift inherent in the nth harmonic of the Fourier series representation of the signal component in the output of the squaring device.

single-pole Butterworth low-pass filter for $H(s)$, the line spectrum at the output of the delay-and-multiply operation was analyzed in [12] as a function of the fractional delay α for both low and high SNRs. In particular, for a given value of SNR and α, it was shown that there exists an optimum filter bandwidth-to-data rate ratio[7] in the sense of minimizing the mean-squared timing error and that the optimum value of α in each case was equal to $1/2$. Furthermore, in addition to $\alpha = 1/2$ optimizing the performance for the best choice of filter bandwidth-to-data rate ratio, it also resulted in a significant improvement in robustness with regard to variations in this ratio.

Although the filter and square symbol synchronizer and its generalization, the cross-spectrum symbol synchronizer, were initially proposed as real baseband schemes that implicitly assumed perfect carrier synchronization, it is straightforward to modify them so as to be useful in a noncoherent carrier phase environment. Specifically, if we now model the signal component of the input in complex form as

$$\tilde{s}(t,\varepsilon) = \sqrt{2P}e^{j\theta_c}\sum_{n=-\infty}^{\infty} d_n p(t - nT - \varepsilon T) \tag{10-64}$$

where θ_c denotes the unknown carrier phase, then performing the delay-and-multiply function in complex conjugate form again will result in a zonal filter output that is a tone at the nth harmonic of the data rate that can be tracked by a PLL. Furthermore, the performance of this scheme will be independent of the value of θ_c. A block diagram of the real noncoherent version of the cross-spectrum synchronizer is illustrated in Fig. 10-12, where the input is now the *bandpass* received signal whose signal component is given by $s(t,\varepsilon) = \mathrm{Re}\left\{\tilde{s}(t,\varepsilon)e^{j\omega_c t}\right\}$ with ω_c denoting the carrier frequency. In what follows, we present the tracking performance of the symbol synchronizer in Fig. 10-12, drawing heavily on the detailed results already contained in [11] and [12].

In accordance with the above, the received bandpass signal is given by

$$\begin{aligned} r(t) &= s(t,\varepsilon) + n(t) \\ &= \sqrt{2P}m(t)\cos(\omega_c t + \theta_c) + \sqrt{2}\left[n_c(t)\cos\omega_c t - n_c(t)\sin\omega_c t\right] \end{aligned} \tag{10-65}$$

where $n_c(t), n_s(t)$ are independent low-pass Gaussian noise processes with single-sided power spectral density N_0 W/Hz. After demodulation with quadrature reference signals

[7] This phenomenon is entirely synergistic with the tracking performance of the Costas or squaring loop as exemplified by its squaring-loss behavior as a function of the ratio of arm filter bandwidth to data rate (see Chapter 8).

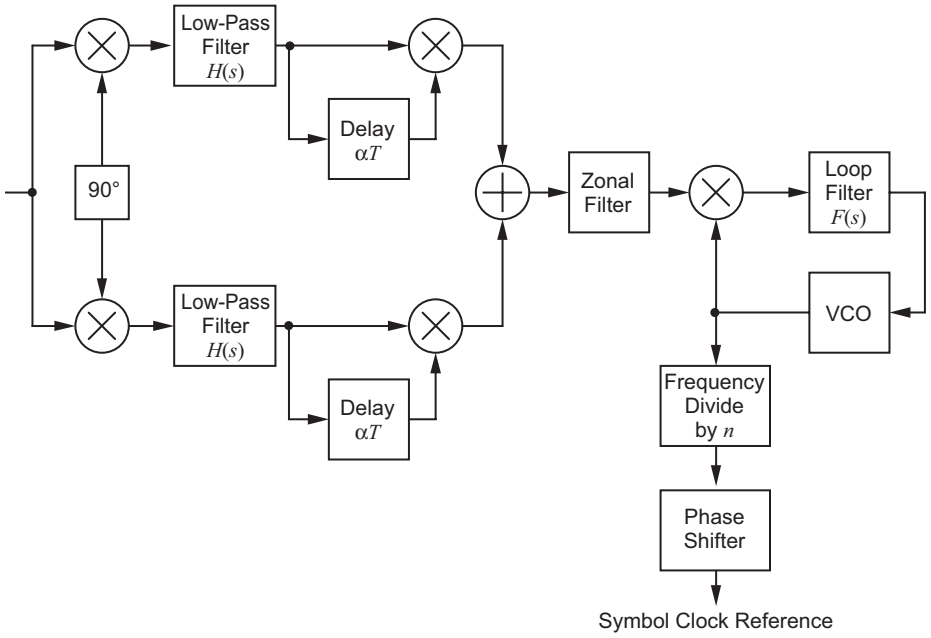

Fig. 10-12. Noncoherent cross-spectrum symbol synchronizer.

$$r_c(t) = \sqrt{2}\cos\omega_c t$$
$$r_s(t) = -\sqrt{2}\sin\omega_c t \tag{10-66}$$

and then filtering and delay-and-multiplying, we obtain the I and Q low-pass signals

$$\begin{aligned}\hat{x}_c(t) &= P\hat{m}(t)\,\hat{m}(t-\alpha T)\cos^2\theta_c + \hat{n}_c(t)\,\hat{n}_c(t-\alpha T)\\ &\quad + \sqrt{P}\cos\theta_c\left[\hat{m}(t)\,\hat{n}_c(t-\alpha T) + \hat{m}(t-\alpha T)\,\hat{n}_c(t)\right]\\ \hat{x}_s(t) &= P\hat{m}(t)\,\hat{m}(t-\alpha T)\sin^2\theta_c + \hat{n}_s(t)\,\hat{n}_s(t-\alpha T)\\ &\quad + \sqrt{P}\sin\theta_c\left[\hat{m}(t)\,\hat{n}_s(t-\alpha T) + \hat{m}(t-\alpha T)\,\hat{n}_s(t)\right]\end{aligned} \tag{10-67}$$

Summing these I and Q signals produces

$$x(t) = P\hat{m}(t)\hat{m}(t-\alpha T) + \hat{n}_c(t)\hat{n}_c(t-\alpha T) + \hat{n}_s(t)\hat{n}_s(t-\alpha T)$$

$$+ \sqrt{P}\hat{m}(t)\left[\hat{n}_c(t-\alpha T)\cos\theta_c + \hat{n}_s(t-\alpha T)\sin\theta_c\right]$$

$$+ \sqrt{P}\hat{m}\,(t-\alpha T)\left[\hat{n}_c(t)\cos\theta_c + \hat{n}_s(t)\sin\theta_c\right] \qquad (10\text{-}68)$$

whose signal × signal ($S \times S$) component [the first term on the right-hand side of Eq. (10-68)] is identical to that of the phase coherent cross-spectral symbol synchronizer and as such is independent of the carrier phase. It now remains to investigate to what extent the noise × noise ($N \times N$) component [the second and third terms on the right-hand side of Eq. (10-68)] and the signal × noise ($S \times N$) component [the fourth and fifth terms on the right-hand side of Eq. (10-68)] have changed and what impact these changes have on the tracking performance of the loop.

As is typical of all synchronization loops of this type, the tracking performance as measured by the mean-squared timing error can be characterized by the "squaring loss," which represents the degradation[8] in this measure due to the nonlinear nature ($S \times S$, $S \times N$, and $N \times N$ operations) of the loop. Specifically, the squaring loss is formed from a scaled version of the ratio of the power in the $S \times S$ component to the equivalent noise power spectral density of the sum of the $S \times N$ and $N \times N$ components, all evaluated at the nth harmonic of the data rate. As we shall see shortly, it will not be necessary to redo the evaluations of these component contributions to the squaring loss from what was done in [11] and [12] for the phase-coherent symbol synchronizer. Rather, we shall simply be able to make direct use of the evaluations found there with simple or no modification at all. As such the evaluation of the squaring loss itself will follow immediately almost by inspection.

To evaluate the equivalent noise power spectral densities of the $S \times N$ and $N \times N$ components, namely, $N'_{0_{S\times N}}$ and $N'_{0_{N\times N}}$, respectively, we must first com-

[8] As we shall see shortly, the squaring loss can at times exceed 0 dB and thus, in reality, can represent a gain rather than a loss. The reason for using such a nomenclature here nonetheless is by analogy with its usage in the carrier sync application, where it represents the additional degradation of the mean-squared *phase* error relative to that of a linear carrier tracking loop such as a PLL, and hence its value there can never exceed 0 dB. The difference between the two usages is centered around the fact that in the carrier sync application the phase error can vary over a range of 2π rad, whereas in the symbol sync application the normalized (to the T-second symbol duration) timing error can vary over a range of unity. Thus, there is a scale factor of $(2\pi)^2$ that comes into play when relating the mean-squared phase error of the sinusoidal clock supplied by the PLL portion of the cross-spectrum symbol synchronizer to the mean-squared normalized timing error of this same reference when used as a symbol sync clock. The important point to keep in mind is that the squaring loss is just a relative measure of performance and thus is useful in comparing different sync schemes.

pute their autocorrelation function. The autocorrelation of the $S \times N$ component is by definition

$$\begin{aligned}
R_{sn}(\tau) =& P\,E\left\{\left[\hat{m}(t)\left[\hat{n}_c(t-\alpha T)\cos\theta_c + \hat{n}_s(t-\alpha T)\sin\theta_c\right]\right.\right. \\
&+\hat{m}(t-\alpha T)\left[\hat{n}_c(t)\cos\theta_c + \hat{n}_s(t)\sin\theta_c\right]\Big] \\
&\times\left[\hat{m}(t+\tau)\left[\hat{n}_c(t-\alpha T+\tau)\cos\theta_c + \hat{n}_s(t-\alpha T+\tau)\sin\theta_c\right]\right. \\
&\left.\left.+\hat{m}(t-\alpha T+\tau)\left[\hat{n}_c(t+\tau)\cos\theta_c + \hat{n}_s(t+\tau)\sin\theta_c\right]\right]\right\} \\
=& 2PR_{\hat{m}}(\tau)\left[R_{\hat{n}_c}(\tau)\cos^2\theta_c + R_{\hat{n}_s}(\tau)\sin^2\theta_c\right] \\
&+ PR_{\hat{m}}(\tau+\alpha T)\left[R_{\hat{n}_c}(\tau-\alpha T)\cos^2\theta_c + R_{\hat{n}_s}(\tau-\alpha T)\sin^2\theta_c\right] \\
&+ PR_{\hat{m}}(\tau-\alpha T)\left[R_{\hat{n}_c}(\tau+\alpha T)\cos^2\theta_c + R_{\hat{n}_s}(\tau+\alpha T)\sin^2\theta_c\right] \qquad (10\text{-}69)
\end{aligned}$$

which after recognizing that $R_{\hat{n}_c}(\tau) = R_{\hat{n}_s}(\tau) = R_{\hat{n}}(\tau)$ simplifies to

$$\begin{aligned}
R_{sn}(\tau) =& P\left[2R_{\hat{m}}(\tau)R_{\hat{n}}(\tau) + R_{\hat{m}}(\tau+\alpha T)R_{\hat{n}}(\tau-\alpha T)\right. \\
&\left.+R_{\hat{m}}(\tau-\alpha T)R_{\hat{n}}(\tau+\alpha T)\right] \qquad (10\text{-}70)
\end{aligned}$$

Again it can be observed that the autocorrelation in Eq. (10-8) is independent of the carrier phase θ_c and furthermore is identical to the analogous result for the phase-coherent cross-spectrum symbol synchronizer as given in Eq. (10) of [12].[9]

Next, the autocorrelation of the $N \times N$ component is obtained as

$$\begin{aligned}
R_{nn}(\tau) =& E\left\{\left[\hat{n}_c(t)\hat{n}_c(t-\alpha T) + \hat{n}_s(t)\hat{n}_s(t-\alpha T)\right]\right. \\
&\left.\times\left[\hat{n}_c(t+\tau)\hat{n}_c(t-\alpha T+\tau) + \hat{n}_s(t+\tau)\hat{n}_s(t-\alpha T+\tau)\right]\right\} \\
=& 2\left[R_{\hat{n}}^2(\alpha T) + R_{\hat{n}}^2(\tau) + R_{\hat{n}}(\tau-\alpha T)R_{\hat{n}}(\tau+\alpha T)\right] \qquad (10\text{-}71)
\end{aligned}$$

[9] Note that the multiplicative factor P has been included here in the definition of $R_{sn}(\tau)$ whereas in [12], where P is denoted by S, it has been erroneously omitted in defining the total noise power spectral density.

which is exactly twice the analogous result for the phase-coherent cross-spectrum symbol synchronizer as given in [12]. Thus, since the equivalent noise power spectral densities are computed from the Fourier transforms of the autocorrelations evaluated at the nth harmonic of the data rate, i.e., $N'_{0_{S\times N}} = 2\int_{-\infty}^{\infty} R_{sn}(\tau)\, e^{j2\pi n\tau/T} d\tau$ and $N'_{0_{N\times N}} = 2\int_{-\infty}^{\infty} R_{nn}(\tau)\, e^{j2\pi n\tau/T} d\tau$, then ignoring the zero frequency term $R_n^2(\alpha T)$ as was done in [12] (since it leads to a power spectral line component at the zeroth harmonic of the data rate which is eliminated by the zonal filter), we conclude that

$$\begin{aligned} N'_{0_{S\times N}}|_{noncoh.} &= N'_{0_{S\times N}}|_{coh.} \\ N'_{0_{N\times N}}|_{noncoh.} &= 2N'_{0_{N\times N}}|_{coh.} \end{aligned} \tag{10-72}$$

Finally, since, as previously stated, the $S \times S$ component of the noncoherent cross-spectral symbol synchronizer is identical to that of the phase coherent one, then letting $|C_n|^2$ denote the normalized power in this component at the nth harmonic of the data rate, the squaring loss of the former is obtained as (see Eq. (48) of [12] with minor corrections applied)

$$\begin{aligned} S_L|_{\text{noncoh.}} &= (2\pi n)^2 PN_0 \left[\frac{2|C_n|^2\Big|_{\text{noncoh.}}}{N'_{0_{S\times N}}\Big|_{\text{noncoh.}} + N'_{0_{N\times N}}\Big|_{\text{noncoh.}}} \right] \\ &= (2\pi n)^2 PN_0 \left[\frac{2|C_n|^2\Big|_{\text{coh.}}}{N'_{0_{S\times N}}\Big|_{\text{coh.}} + 2N'_{0_{N\times N}}\Big|_{\text{coh.}}} \right] \end{aligned} \tag{10-73}$$

At this point, it is straightforward to evaluate Eq. (10-73) by making use of the expressions in [12] for $|C_n|^2\big|_{\text{coh.}}$, $N'_{0_{S\times N}}\big|_{\text{coh.}}$, and $N'_{0_{N\times N}}\big|_{coh.}$. A summary of these results for the special case of a single-pole Butterworth low-pass filter for $H(s)$ (with 3-dB cutoff frequency f_c), random (transition density equal to 0.5) NRZ data, $n = 1$ (tracking of the first harmonic), and either $\alpha = 0$ (the filter and square-law implementation) or $\alpha = 0.5$ (a half-symbol delay that was shown in [12] to be optimum in the sense of minimizing the squaring loss at the best ratio of low-pass filter bandwidth to symbol time) is given in the following.[10]

[10] These results were not explicitly given in [12] but have been independently derived here after considerable manipulation and integral evaluation.

For $\alpha = 0$:

$$|C_1|^2 = \frac{\left[1 - \exp(-2\pi R)\right]^2}{(2\pi R)^2} \frac{1}{[1 + 1/R^2][1 + 1/4R^2]}$$

$$N'_{0_{S\times N}}\Big|_{\text{coh.}} = \frac{4PN_0}{1 + 1/R^2}\left\{1 - \frac{1 - \exp(-2\pi R)}{8\pi R}\left[\frac{6 + 1/R^2 + 1/R^4}{[1 + 1/R^2][1 + 1/4R^2]}\right]\right\} \quad (10\text{-}74)$$

$$N'_{0_{N\times N}}\Big|_{\text{coh.}} = \frac{PN_0}{1 + 1/4R^2}\left(\frac{\pi R}{2E_s/N_0}\right)$$

For $\alpha = 0.5$:

$$|C_1|^2 = \frac{1}{(2\pi)^2[1 + 1/R^2][1 + 1/4R^2]} \times \left\{\frac{\left[\exp(-\pi R)\left[3 - \exp(-2\pi R)\right] - 2\right]^2}{4R^2} + 4\right\}$$

$$N'_{0_{S\times N}}\Big|_{\text{coh.}} = \frac{2PN_0}{1 + 1/R^2}\left\{1 - \frac{1}{4\pi R}\left[\frac{1 - 1/R^2}{1 + 1/R^2} + \frac{1}{2}\left(\frac{1 + 1/R^2}{1 + 1/4R^2}\right)\right]\left[3 - 4\exp(-2\pi R) + \exp(-4\pi R)\right]\right\} \quad (10\text{-}75)$$

$$N'_{0_{N\times N}}\Big|_{\text{coh.}} = \frac{PN_0}{1 + 1/4R^2}\left(\frac{\pi R}{4E_s/N_0}\right)\left[1 - \exp(-2\pi R)\right]$$

where $R \triangleq f_c T$ and $E_s = PT$ is the symbol energy.

Figure 10-13 is an illustration of $S_L\big|_{\text{noncoh.}}$ as computed from Eq. (10-73) together with Eq. (10-74) or Eq. (10-75) versus R with E_s/N_0 as a parameter. Also shown in dashed lines are the corresponding plots of the squaring-loss performance for the coherent cross-spectrum symbol synchronizer, namely $S_L\big|_{\text{coh.}}$, as previously obtained in [12] or equivalently from Eq. (10-73) by ignoring the factor of two in front of $N'_{0_{N\times N}}\big|_{\text{coh.}}$. We observe that the noncoherent symbol synchronizer performs almost as well as the coherent one at high SNR (where the $S \times N$ noise dominates over the $N \times N$ noise), whereas at low SNR (where the $N \times N$ noise dominates over the $S \times N$ noise) there is a more significant degradation of the former relative to the latter. Next, as was the case for the coherent symbol synchronizers, the noncoherent cross-spectrum scheme with

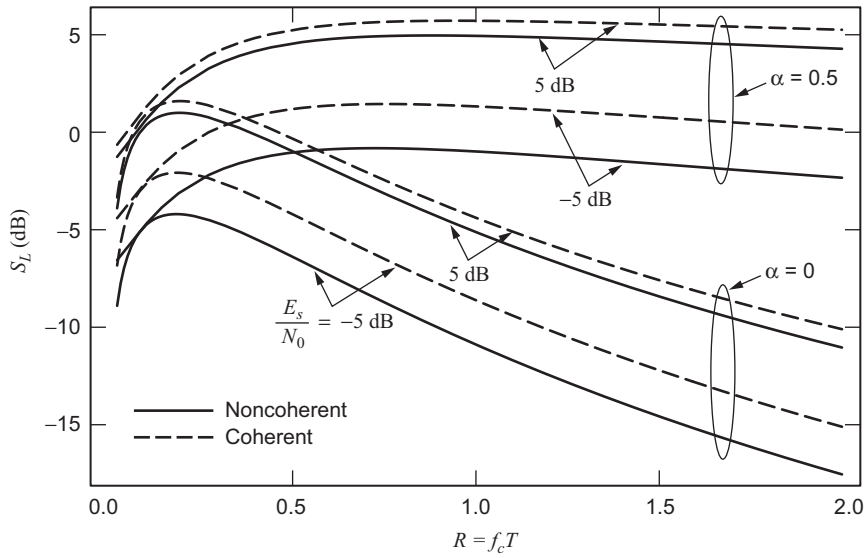

Fig. 10-13. Squaring-loss performance of noncoherent and coherent cross-spectrum symbol synchronizers.

half-symbol delay provides an improvement in performance over the filter and square-law scheme when implemented with the optimum value of bandwidth–time product R. Furthermore, although the cross-spectrum schemes exhibit a dependence on the bandwidth–time product for all values of α, this dependence is considerably reduced by the use of a half-symbol delay, particularly when compared with that for $\alpha = 0$.

To explain the much slower roll-off of the squaring loss performance with R for the half-symbol delay case, we reason as follows. In the limit of large low-pass filter bandwidth (theoretically no filtering at all), when $\alpha = 0$ the signal component of the output of the delay-and-multiply circuit (equivalent to a squaring operation in this case) is a squared NRZ waveform which simply is a constant equal to unity and as such does not contain a harmonic at $1/T$. This is born out by the fact that the normalized signal power of the harmonic at $1/T$ as given by $|C_1|^2$ in Eq. (10-74) is equal to zero in the limit of $R \to \infty$. On the other hand, in the same limit with $\alpha = 0.5$, the output of the delay-and-multiply circuit randomly alternates between a ± 1 square wave at the data rate and a $+1$ constant. The average of these two waveforms is a unipolar $(0, 1)$ square wave at the data rate whose Fourier series expansion clearly contains a nonzero harmonic at $1/T$. Once again this is born out by the fact that, using Eq. (10-75), in the limit of $R \to \infty$ and $E_s/N_0 \to \infty$ we have $|C_1|^2 = 1/\pi^2$. Since, for large R, the $N'_{0_{N\times N}}\big|_{\text{coh.}}$ term dominates over the $N'_{0_{S\times N}}\big|_{\text{coh.}}$ and since for $\alpha = 0$ and $\alpha = 0.5$ they both have the same behavior (except for a factor of two smaller

for the latter), then when taking the ratio of $|C_1|^2$ to the sum of $N'_{0_{S\times N}}\big|_{\text{coh.}}$ and $N'_{0_{N\times N}}\big|_{\text{coh.}}$, the squaring loss for the half-symbol delay case will decay with R much less rapidly than for the zero-delay (squaring) case.

It is now of interest to compare the performance of the noncoherent cross-spectrum symbol synchronizers to that of the coherent DTTL whose squaring loss is obtained from Eq. (10-40) using the relation $\sigma_\lambda^2 = 1/\rho S_L$, i.e.,

$$S_L = \frac{2\left[\text{erf}\left(\sqrt{\frac{E_s}{N_0}}\right) - \frac{\xi}{2}\sqrt{\frac{E_s/N_0}{\pi}}\exp\left(-\frac{E_s}{N_0}\right)\right]^2}{\xi\left\{1 + \frac{\xi}{2}\left(\frac{E_s}{N_0}\right) - \frac{\xi}{2}\left[\frac{1}{\sqrt{\pi}}\exp\left(-\frac{E_s}{N_0}\right) + \sqrt{\frac{E_s}{N_0}}\,\text{erf}\left(\sqrt{\frac{E_s}{N_0}}\right)\right]^2\right\}} \tag{10-76}$$

Figures 10-14(a) and 10-14(b) are plots of the squaring loss given by Eq. (10-76) versus E_s/N_0 in dB and, for comparison, the optimum (with respect to choice of R) squaring loss for the coherent and noncoherent cross-spectrum schemes corresponding to $\alpha = 0$ and $\alpha = 0.5$, respectively. In the case of Fig. 10-14(a), we observe that, regardless of its window width, the DTTL outperforms the noncoherent cross-spectrum (filter and square) scheme over the entire range of SNR illustrated. On the other hand, when compared to the coherent cross-spectrum scheme, for sufficiently large window width, the DTTL performance will suffer a degradation at low values of SNR. This should not be surprising since, as mentioned earlier in the chapter, the DTTL is derived from a high SNR approximation to the MAP symbol synchronizer which itself is motivated by the MAP estimation approach only in the limit of infinitesimally small window width.[11] With reference to Fig. 10-14(b), we observe that the performance of the coherent cross-spectrum scheme is quite competitive with that of the DTTL having a window width $\xi = 0.5$, and even the noncoherent cross-spectrum scheme can slightly outperform this DTTL at high SNR. As the window width is increased beyond a value of one-half, the cross-spectrum symbol sync schemes will clearly outperform the DTTL over the entire range of SNRs.

[11] The window width, ξ, of the DTTL corresponds to the approximation of the derivative of an NRZ pulse at a transition point in the data stream, namely, a delta function, with a finite-width rectangular pulse. Thus, the validity of the approximation, as well as the tracking performance of the closed-loop DTTL, monotonically improves as the window width becomes smaller and smaller. However, while in principle the MAP approach suggests an infinitesimally small window width, in practice there is a lower limit on its value since the width of the tracking region is directly proportional to ξ. Thus, if the window width is made too small, the ability of the loop to remain in lock will severely diminish. The choice of window width is determined by the condition $\sigma_\lambda \ll \xi$.

While it is difficult analytically to obtain the limiting behavior of the cross-spectrum schemes when E_s/N_0 approaches infinity, it can be shown numerically that, for both the noncoherent and coherent versions, the optimum value of R is approximately equal to 1.1, and the accompanying value of squaring loss is 6.84 dB.

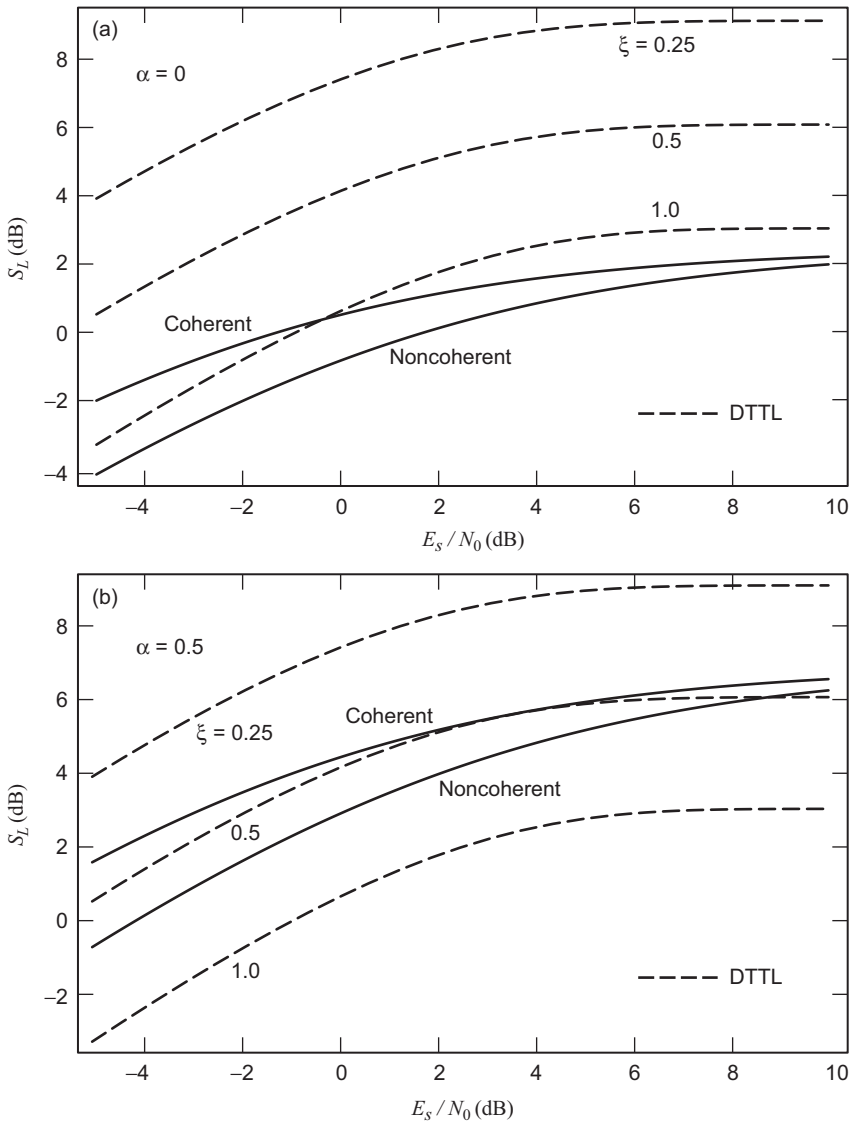

Fig. 10-14. A comparison of the squaring-loss performance of noncoherent and coherent cross-spectrum symbol synchronizers with that of the DTTL: (a) $\alpha = 0$ and (b) $\alpha = 0.5$.

10.6.2 The Noncoherent DTTL

In this section, we return to the ML approach for obtaining a symbol synchronizer in the absence of carrier phase information with particular emphasis on the necessary modifications of the conventional (coherent) DTTL structures as treated earlier in this chapter. We shall see that, in the low SNR region, the modification resembles that found for the suboptimum schemes discussed in the previous subsection, i.e., the independent addition of the symbol sync component derived from the quadrature carrier arm, whereas for the high SNR region, the structure involves a nonlinear cross-coupling of symbol sync components from both the in-phase and quadrature carrier arms. Wherever possible, results will be obtained from a combination of theory and simulation. Before proceeding, it should be mentioned that the MAP approach to symbol sync was considered in [13] in the context of arriving at a non-data-aided recursive algorithm for symbol timing. Although at first glance it might appear that the approach taken there corresponds to noncoherent symbol sync since the carrier phase was assumed to be unknown but independent from symbol to symbol,[12] in reality the derivation of the MAP estimate of symbol sync was preceded by a recursive estimate of the carrier phase which justifies such an assumption. Our emphasis here, as mentioned above, is on interpreting the likelihood function derived from such an approach in such a way as to arrive at noncoherent versions of the DTTL. For the sake of brevity and consistent with the original derivation of the coherent DTTL, we shall focus only on the BPSK ($M = 2$), NRZ case.

10.6.2.1 MAP Symbol Sync Estimation in the Absence of Carrier Phase Information. The input to the receiver is a bandpass signal modeled by the combination of Eq. (10-65) together with Eq. (10-64). The first step is to demodulate the received signal with the quadrature carrier reference signals

$$\begin{aligned} r_c(t) &= \sqrt{2}\cos\omega_c t \\ r_s(t) &= -\sqrt{2}\sin\omega_c t \end{aligned} \tag{10-77}$$

resulting in the pair of baseband observables in the nth symbol interval $(n+\varepsilon)T \leq t \leq (n+1+\varepsilon)T$

[12] As we shall see shortly, the appropriate assumption for truly noncoherent symbol sync is an unknown carrier phase that is constant over the duration of the observation, i.e., a sequence of symbols.

$$\begin{aligned} x_{cn}(t) &= \sqrt{P} d_n p\big(t-(n+\varepsilon)T\big)\cos\theta_c + n_c(t)\cos\theta_c - n_s(t)\sin\theta_c \\ &= s(t,\varepsilon,d_n)\cos\theta_c + n_{cn}(t,\theta_c) \\ x_{sn}(t) &= \sqrt{P} d_n p\big(t-(n+\varepsilon)T\big)\sin\theta_c + n_c(t)\sin\theta_c + n_s(t)\cos\theta_c \\ &= s(t,\varepsilon,d_n)\sin\theta_c + n_{sn}(t,\theta_c) \end{aligned} \tag{10-78}$$

or, equivalently, in complex form,

$$\tilde{x}_n(t) = x_{cn}(t) + j x_{sn}(t) = s(t,\varepsilon,d_n)\, e^{j\theta_c} + \tilde{n}_n(t,\theta_c) \tag{10-79}$$

where

$$\begin{aligned} \tilde{n}_n(t,\theta) &= n_{cn}(t) + j n_{sn}(t) = \tilde{n}_n(t) e^{j\theta_c} \\ \tilde{n}_n(t) &= n_c(t) + j n_s(t) \end{aligned} \tag{10-80}$$

Then, for an observation of duration $T_0 = NT$ seconds, i.e., N iid symbols, the CLF (conditioning is now on both the unknown carrier phase θ_c and fractional symbol timing offset ε) is given by

$$\begin{aligned} L(\mathbf{d},\varepsilon,\theta_c) &= \frac{1}{\pi N_0}\exp\left(-\frac{1}{N_0}\int_{T_0}\left|\tilde{x}(t) - s(t,\varepsilon,\mathbf{d})\, e^{j\theta_c}\right|^2 dt\right) \\ &= C\exp\left(\frac{2}{N_0}\,\mathrm{Re}\left\{\int_{T_0}\tilde{x}(t)\, s(t,\varepsilon,\mathbf{d})\, e^{-j\theta_c} dt\right\}\right) \end{aligned} \tag{10-81}$$

where $\tilde{x}(t) = \big(\tilde{x}_1(t), \tilde{x}_2(t), \cdots, \tilde{x}_N(t)\big)$ is the collection of complex observables and C is a constant that is independent of the unknown parameters and also reflects the constant energy nature of the BPSK modulation. As before, because of the iid property of the data symbols, the CLF can be expressed as the product of per-symbol CLFs, namely,

$$L(\mathbf{d},\varepsilon,\theta_c) = \prod_{n=0}^{N-1}\exp\left(\frac{2}{N_0}\,\mathrm{Re}\left\{\int_{T_n(\varepsilon)}\tilde{x}_n(t)\, s(t,\varepsilon,d_n)\, e^{-j\theta_c} dt\right\}\right) \tag{10-82}$$

where $T_n(\varepsilon)$ denotes the time interval $(n+\varepsilon)T \le t \le (n+1+\varepsilon)T$ and for simplicity we have ignored all multiplicative constants since they do not affect the parameter estimation.

The issue that arises now is the order in which to perform the averaging over the unknown data sequence and the unknown carrier phase. Suppose that one attempts to first average over the carrier phase. In order to do this, we rewrite Eq. (10-82) in the form

$$L(\mathbf{d},\varepsilon,\theta_c) = \exp\left(\frac{2}{N_0}\,\mathrm{Re}\left\{\sum_{n=1}^{N}\int_{T_n(\varepsilon)} \tilde{x}_n(t)\, s(t,\varepsilon,d_n)\, e^{-j\theta_c} dt\right\}\right)$$

$$= \exp\left\{\frac{2}{N_0} R(\mathbf{d},\varepsilon)\cos\left[\theta_c - \alpha(\mathbf{d},\varepsilon)\right]\right\} \tag{10-83}$$

where

$$R(\mathbf{d},\varepsilon) = \left|\sum_{n=0}^{N-1}\int_{T_n(\varepsilon)} \tilde{x}_n(t) s(t,\varepsilon,d_n) dt\right|$$

$$= \left|\sum_{n=0}^{N-1} d_n\sqrt{P}\int_{T_n(\varepsilon)} \tilde{x}_n(t) p\big(t-(n+\varepsilon)T\big) dt\right| \tag{10-84}$$

$$\alpha(\mathbf{d},\varepsilon) = \arg\left\{\sum_{n=0}^{N-1}\int_{T_n(\varepsilon)} \tilde{x}_n(t) s(t,\varepsilon,d_n) dt\right\}$$

Averaging over the uniformly distributed carrier phase, we get[13]

$$L(\mathbf{d},\varepsilon) = I_0\left(\frac{2}{N_0} R(\mathbf{d},\varepsilon)\right)$$

$$= I_0\left(\frac{2\sqrt{P}}{N_0}\left|\sum_{n=0}^{N-1} d_n \int_{T_n(\varepsilon)} \tilde{x}_n(t)\, p\big(t-(n+\varepsilon)T\big) dt\right|\right) \tag{10-85}$$

[13] At this point, it should be re-emphasized that our approach differs from that in [13] in that in the latter the *per symbol* likelihood function is averaged over the carrier phase and then, because of the iid nature of the data, an LF is formed from the product of these phase-averaged LFs. Forming the LF in such a way implicitly assumes that the carrier phase varies independently from symbol to symbol, which is in opposition to our assumption that the carrier phase is constant over the observation.

The difficulty now lies in analytically averaging over the data sequence in Eq. (10-85) when N is large. Thus, in order to obtain simple metrics, before averaging over the data, we must first simplify matters by approximating the nonlinear (Bessel) function in Eq. (10-85). For small arguments (e.g., low SNR), the following approximation is appropriate:

$$I_0(x) \cong 1 + \frac{x^2}{4} \tag{10-86}$$

Applying Eq. (10-86) to Eq. (10-85) and defining the real observables

$$\begin{aligned} X_{cn}(\varepsilon) &\triangleq \int_{T_n(\varepsilon)} \tilde{x}_{cn}(t)\, p\big(t-(n+\varepsilon)T\big)dt \\ X_{sn}(\varepsilon) &\triangleq \int_{T_n(\varepsilon)} \tilde{x}_{sn}(t)\, p\big(t-(n+\varepsilon)T\big)dt \end{aligned} \tag{10-87}$$

we obtain

$$\begin{aligned} L(\mathbf{d},\varepsilon) &= I_0\left(\frac{2\sqrt{P}}{N_0}\left|\sum_{n=0}^{N-1} d_n\big(X_{cn}(\varepsilon)+jX_{sn}(\varepsilon)\big)\right|\right) \\ &\cong 1+\frac{P}{N_0^2}\left(\sum_{n=0}^{N-1} d_n X_{cn}(\varepsilon)\right)^2+\frac{P}{N_0^2}\left(\sum_{n=0}^{N-1} d_n X_{sn}(\varepsilon)\right)^2 \end{aligned} \tag{10-88}$$

Finally, averaging over the iid data sequences gives the simplified LF

$$L(\varepsilon) = 1+\frac{P}{N_0^2}\sum_{n=0}^{N-1} X_{cn}^2(\varepsilon)+\frac{P}{N_0^2}\sum_{n=0}^{N-1} X_{sn}^2(\varepsilon) \tag{10-89}$$

To arrive at a closed-loop symbol sync structure motivated by this LF, we proceed in the usual way by differentiating the LF with respect to ε and using the result to form the error signal in the loop. Taking the partial derivative of Eq. (10-89) with respect to ε and again ignoring multiplicative constants gives

$$\frac{\partial L(\varepsilon)}{\partial \varepsilon} = \sum_{n=0}^{N-1} X_{cn}(\varepsilon)\frac{dX_{cn}(\varepsilon)}{d\varepsilon}+X_{sn}(\varepsilon)\frac{dX_{sn}(\varepsilon)}{d\varepsilon} \tag{10-90}$$

each of whose terms is analogous to that which forms the error signal in the low SNR version of the coherent DTTL, i.e., the LDTTL. Thus, the low SNR version of the noncoherent DTTL, herein given the acronym NC-LDTTL, is nothing more than the parallel combination of two independent coherent LDTTLs acting on the I and Q baseband signals. A block diagram of this structure is given in Fig. 10-15, and the analysis of its performance will follow in the next subsection.

For large SNR, we need to approximate $I_0(x)$ in Eq. (10-85) by its large argument form, which behaves as $\exp(|x|)$. Thus, in this case the CLF would be approximated as

$$L(\mathbf{d},\varepsilon) \cong \exp\left(\frac{2\sqrt{P}}{N_0}\left|\sum_{n=0}^{N-1} d_n \int_{T_n(\varepsilon)} \tilde{x}_n(t)\, p\big(t-(n+\varepsilon)T\big)dt\right|\right) \tag{10-91}$$

which unfortunately does not ease the burden of averaging over the data sequence.

Suppose now instead we first average the CLF over the data. Then from Eq. (10-82) we have

$$\begin{aligned} L(\varepsilon,\theta_c) &= \underset{\mathbf{d}}{E}\left\{\prod_{n=0}^{N-1}\exp\left(\frac{2}{N_0}\operatorname{Re}\left\{\int_{T_n(\varepsilon)} \tilde{x}_n(t)\, s(t,\varepsilon,d_n)\, e^{-j\theta_c}dt\right\}\right)\right\} \\ &= \prod_{n=0}^{N-1}\underset{d_n}{E}\left\{\exp\left(d_n\frac{2\sqrt{P}}{N_0}\operatorname{Re}\left\{\int_{T_n(\varepsilon)} \tilde{x}_n(t)\, p\big(t-(n+\varepsilon)T\big)e^{-j\theta_c}dt\right\}\right)\right\} \\ &= \prod_{n=0}^{N-1}\cosh\left(\frac{2\sqrt{P}}{N_0}\left[X_{cn}(\varepsilon)\cos\theta_c + X_{sn}(\varepsilon)\sin\theta_c\right]\right) \\ &= \prod_{n=0}^{N-1}\cosh\left(\frac{2\sqrt{P}}{N_0}\sqrt{\big(X_{cn}(\varepsilon)\big)^2+\big(X_{sn}(\varepsilon)\big)^2}\cos(\theta_c-\beta_n)\right) \end{aligned} \tag{10-92}$$

where

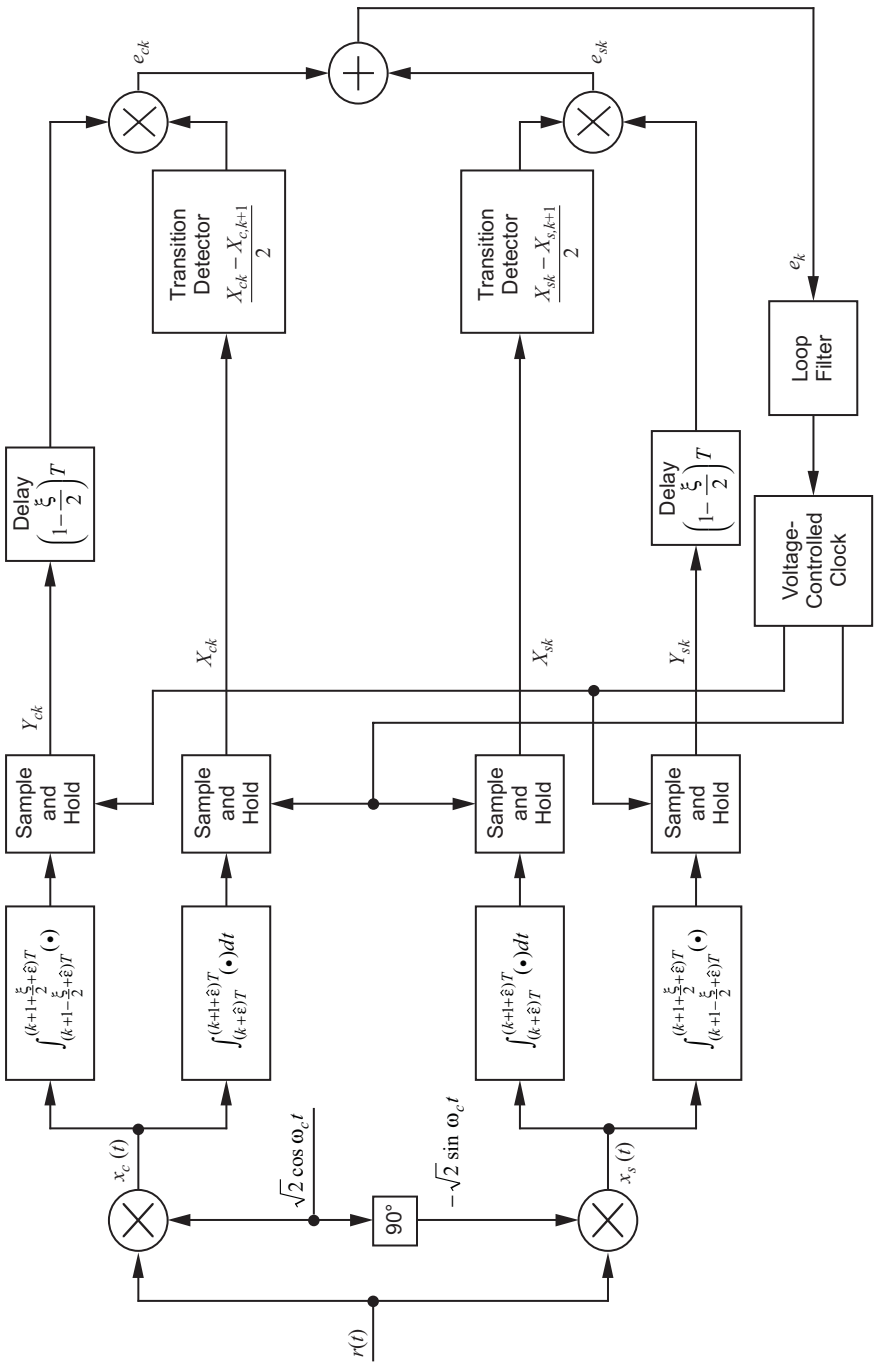

Fig. 10-15. Noncoherent linear data transition tracking loop (NC-LDTTL).

$$\beta_n = \tan^{-1} \frac{X_{sn}(\varepsilon)}{X_{cn}(\varepsilon)} \tag{10-93}$$

If we now apply the large argument (e.g., high SNR) approximation to the hyperbolic cosine function, namely,

$$\cosh x \cong \frac{\exp(|x|)}{2} \tag{10-94}$$

then Eq. (10-92) becomes (ignoring multiplicative constants)

$$L(\varepsilon, \theta_c) = \exp\left\{ \sum_{n=0}^{N-1} \left| \frac{2\sqrt{P}}{N_0} \sqrt{\big(X_{cn}(\varepsilon)\big)^2 + \big(X_{sn}(\varepsilon)\big)^2} \cos(\theta_c - \beta_n) \right| \right\} \tag{10-95}$$

which still presents difficulty in analytically averaging over the unknown parameter, in this case θ_c. Thus, having failed on both attempts at averaging the CLF over *both* the carrier phase and the data sequence at high SNR, we are forced to deviate from the true ML approach in favor of one that will provide a simple metric.

Another approach, albeit suboptimum, that can achieve near-ML performance is to choose (rather than average over) the value of the unknown parameter that maximizes the CLF. With reference to Eq. (10-85), in the limit of no noise (infinite SNR), the CLF $L(\mathbf{d}, \varepsilon)$, or equivalently the argument of the Bessel function, would be maximized when

$$d_n = \operatorname{sgn}\left[\int_{T_n(\varepsilon)} s(t, \varepsilon, d_n) p\big(t - (n+\varepsilon)T\big) dt \right] \tag{10-96}$$

i.e., all the signal vectors are aligned in the same direction, in which case the argument of the Bessel function (ignoring the constant multiplicative factor) would become

$$\left|\sum_{n=1}^{N} d_n \int_{T_n(\varepsilon)} s(t,\varepsilon,d_n) e^{j\theta_c} p\big(t-(n+\varepsilon)T\big)dt\right| =$$

$$\sum_{n=1}^{N}\left|\int_{T_n(\varepsilon)} s(t,\varepsilon,d_n) e^{j\theta_c} p\big(t-(n+\varepsilon)T\big)dt\right|$$

Thus, as a high SNR approximation of this limiting case, we propose the ad hoc unconditional LF

$$\mathrm{LF}(\varepsilon) = I_0\left(\frac{2\sqrt{P}}{N_0}\sum_{n=0}^{N-1}\left|\int_{T_n(\varepsilon)} \tilde{x}_n(t)\, p\big(t-(n+\varepsilon)\,T\big)dt\right|\right) \tag{10-97}$$

or, equivalently, taking the natural logarithm of Eq. (10-97), the log-likelihood function (LLF)

$$\begin{aligned}\mathrm{LLF}(\varepsilon) = \ln \mathrm{LF}(\varepsilon) &= \ln I_0\left(\frac{2\sqrt{P}}{N_0}\sum_{n=0}^{N-1}\left|\int_{T_n(\varepsilon)} \tilde{x}_n(t) p\big(t-(n+\varepsilon)T\big)dt\right|\right)\\ &= \ln I_0\left(\frac{2\sqrt{P}}{N_0}\sum_{n=0}^{N-1}\left|X_{cn}(\varepsilon)+jX_{sn}(\varepsilon)\right|\right)\\ &= \ln I_0\left(\frac{2\sqrt{P}}{N_0}\sum_{n=0}^{N-1}\sqrt{X_{cn}^2(\varepsilon)+X_{sn}^2(\varepsilon)}\right)\end{aligned} \tag{10-98}$$

For large arguments, the nonlinearity in Eq. (10-98) can be approximated (to within a scaling constant) as

$$\ln I_0(x) \cong |x| \tag{10-99}$$

which after substitution in Eq. (10-98) yields

$$\mathrm{LLF}(\varepsilon) = \frac{2\sqrt{P}}{N_0}\sum_{n=0}^{N-1}\sqrt{X_{cn}^2(\varepsilon)+X_{sn}^2(\varepsilon)} \tag{10-100}$$

Thus, analogous to Eq. (10-90), differentiating LLF(ε) with respect to ε, the error signal in a closed-loop configuration should be formed from

$$e = \sum_{n=0}^{N-1} \left[\frac{X_{cn}(\varepsilon)}{\sqrt{X_{cn}^2(\varepsilon) + X_{sn}^2(\varepsilon)}} \frac{dX_{cn}(\varepsilon)}{d\varepsilon} + \frac{X_{sn}(\varepsilon)}{\sqrt{X_{cn}^2(\varepsilon) + X_{sn}^2(\varepsilon)}} \frac{dX_{sn}(\varepsilon)}{d\varepsilon} \right] \tag{10-101}$$

A noncoherent DTTL-type symbol synchronizer that is motivated by using Eq. (10-101) as its error signal is illustrated in Fig. 10-16. The analysis of its performance will be discussed later on. In the meantime it is interesting to note that if one were to consider the coherent case wherein $X_{sn}(\varepsilon)$ would be absent, then setting $X_{sn}(\varepsilon)$ equal to zero in Eq. (10-101) gives

$$e = \sum_{n=0}^{N-1} \frac{X_{cn}(\varepsilon)}{\sqrt{X_{cn}^2(\varepsilon)}} \frac{dX_{cn}(\varepsilon)}{d\varepsilon} = \sum_{n=0}^{N-1} \frac{dX_{cn}(\varepsilon)}{d\varepsilon} \operatorname{sgn} X_{cn}(\varepsilon) \tag{10-102}$$

which is exactly the error signal that would be derived from the MAP approach under the assumption of perfectly known carrier phase and thus motivates the construction of the conventional nonlinear DTTL.

Before proceeding, it is interesting at this point to note that the LLF in Eq. (10-98) is the same[14] as that given in [13, Eq. 6.279], which is obtained by averaging over the carrier phase under the assumption that it varies independently from symbol to symbol as discussed in Footnote 13. The LLF in Eq. (10-98) can also be obtained from Eq. (10-95) by again assuming that the carrier phase varies independently from symbol to symbol, which is tantamount to replacing θ_c with θ_{cn} in this equation, and then *maximizing* over the sequence of carrier phases. It is clear from Eq. (10-95) that this maximization would occur for $\theta_{cn} = \beta_n$, in which case we obtain the LF

$$L(\varepsilon) = \exp\left\{ \sum_{n=0}^{N-1} \left| \frac{2\sqrt{P}}{N_0} \sqrt{\left(X_{cn}(\varepsilon)\right)^2 + \left(X_{sn}(\varepsilon)\right)^2} \right| \right\} \tag{10-103}$$

[14] The only difference is a factor of $\sqrt{T}$ in the argument of the Bessel function, i.e., $2\sqrt{P}/N_0$ in our result versus $2\sqrt{E}/N_0 = 2\sqrt{PT}/N_0$ in that of [13], which comes about because of the difference in the normalization of the carrier reference signals between the two approaches.

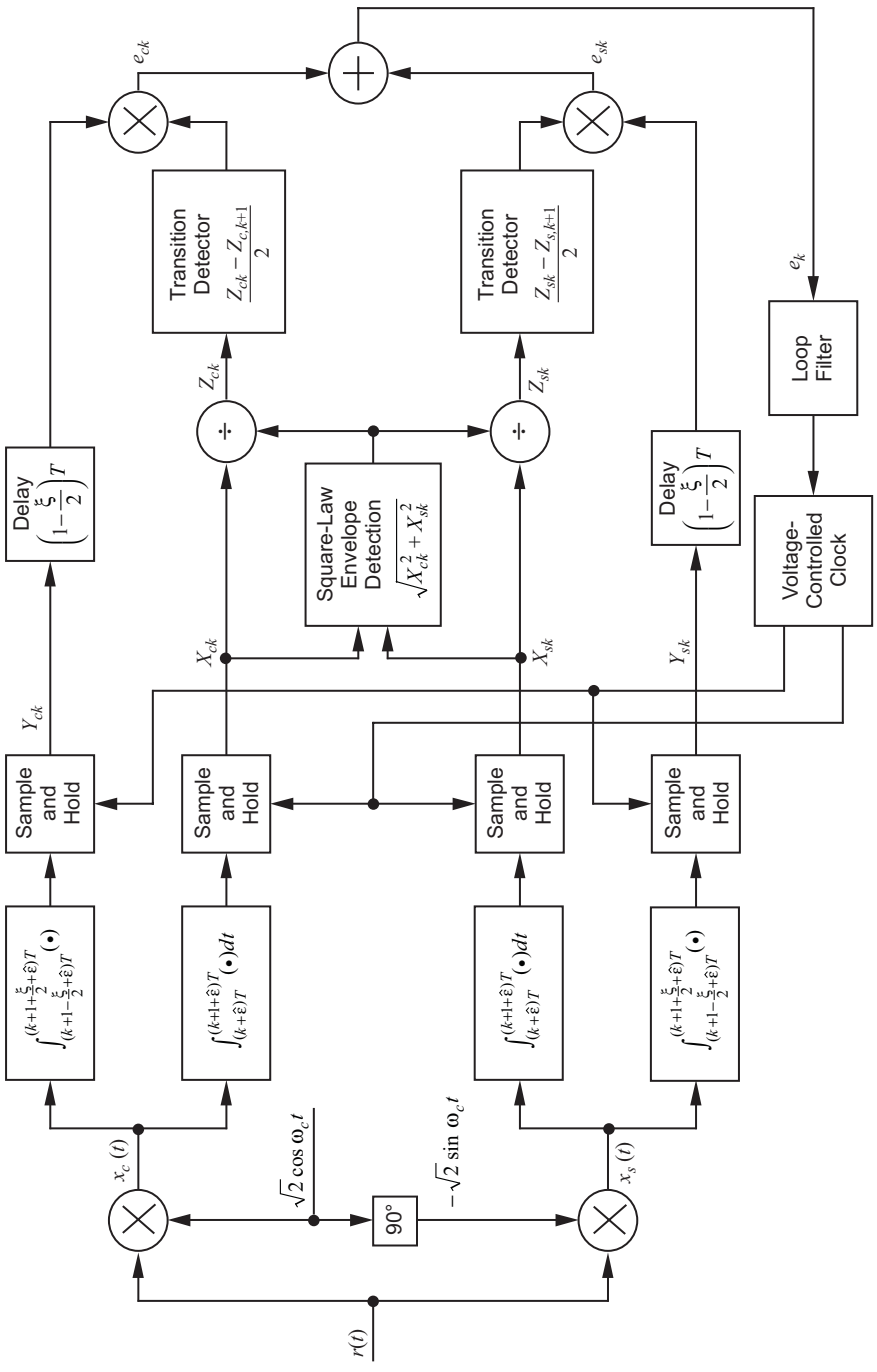

Fig. 10-16. Noncoherent nonlinear data transition tracking loop (NC-NLDTTL).

Finally, taking the natural logarithm of Eq. (10-103) produces a result identical to Eq. (10-100) for the LLF.

10.6.2.2 Tracking Performance of the Noncoherent Linear DTTL. With reference to Fig. 10-15, the upper and lower channel (herein referred to as "cosine" and "sine" channels) inputs to the I&D filters in the nth symbol interval are described by Eq. (10-78). The local clock produces a timing reference for the I and Q I&D filters of each of these channels that depends on the estimate $\hat{\varepsilon}$ of ε. As such, the outputs of these same filters are respectively given by (assuming for simplicity that all gains are set equal to unity)

$$\begin{aligned} X_{ck} &= \int_{kT+\hat{\varepsilon}}^{(k+1)T+\hat{\varepsilon}} x_{ck}(t)dt \\ &= \cos\theta_c \overbrace{\int_{kT+\hat{\varepsilon}}^{(k+1)T+\hat{\varepsilon}} s(t,\varepsilon,d_k)dt}^{c_k} + \cos\theta_c \overbrace{\int_{kT+\hat{\varepsilon}}^{(k+1)T+\hat{\varepsilon}} n_c(t)\,dt}^{\nu_{ck}} \\ &\quad - \sin\theta_c \overbrace{\int_{kT+\hat{\varepsilon}}^{(k+1)T+\hat{\varepsilon}} n_s(t)\,dt}^{\nu_{sk}} \end{aligned} \tag{10-104}$$

$$\begin{aligned} Y_{ck} &= \int_{(k+1-\frac{\xi}{2})T+\hat{\varepsilon}}^{(k+1+\frac{\xi}{2})T+\hat{\varepsilon}} x_{ck}(t)dt \\ &= \cos\theta_c \overbrace{\int_{(k+1-\frac{\xi}{2})T+\hat{\varepsilon}}^{(k+1+\frac{\xi}{2})T+\hat{\varepsilon}} s(t,\varepsilon,d_k)dt}^{b_k} + \cos\theta_c \overbrace{\int_{(k+1-\frac{\xi}{2})T+\hat{\varepsilon}}^{(k+1+\frac{\xi}{2})T+\hat{\varepsilon}} n_c(t)\,dt}^{\mu_{ck}} \\ &\quad - \sin\theta_c \overbrace{\int_{(k+1-\frac{\xi}{2})T+\hat{\varepsilon}}^{(k+1+\frac{\xi}{2})T+\hat{\varepsilon}} n_s(t)\,dt}^{\mu_{sk}} \end{aligned}$$

and

$$
\begin{aligned}
X_{sk} &= \int_{kT+\hat{\varepsilon}}^{(k+1)T+\hat{\varepsilon}} x_{sk}(t)dt \\
&= \sin\theta_c \overbrace{\int_{kT+\hat{\varepsilon}}^{(k+1)T+\hat{\varepsilon}} s(t,\varepsilon,d_k)dt}^{c_k} + \sin\theta_c \overbrace{\int_{kT+\hat{\varepsilon}}^{(k+1)T+\hat{\varepsilon}} n_c\left(t\right)dt}^{\nu_{ck}} \\
&\quad + \cos\theta_c \overbrace{\int_{kT+\hat{\varepsilon}}^{(k+1)T+\hat{\varepsilon}} n_s\left(t\right)dt}^{\nu_{sk}}
\end{aligned}
\tag{10-105}
$$

$$
\begin{aligned}
Y_{sk} &= \int_{(k+1-\frac{\xi}{2})T+\hat{\varepsilon}}^{(k+1+\frac{\xi}{2})T+\hat{\varepsilon}} x_{sk}(t)dt \\
&= \sin\theta_c \overbrace{\int_{(k+1-\frac{\xi}{2})T+\hat{\varepsilon}}^{(k+1+\frac{\xi}{2})T+\hat{\varepsilon}} s(t,\varepsilon,d_k)dt}^{b_k} + \sin\theta_c \overbrace{\int_{(k+1-\frac{\xi}{2})T+\hat{\varepsilon}}^{(k+1+\frac{\xi}{2})T+\hat{\varepsilon}} n_c\left(t\right)dt}^{\mu_{ck}} \\
&\quad + \cos\theta_c \overbrace{\int_{(k+1-\frac{\xi}{2})T+\hat{\varepsilon}}^{(k+1+\frac{\xi}{2})T+\hat{\varepsilon}} n_s\left(t\right)dt}^{\mu_{sk}}
\end{aligned}
$$

Since μ_{ck} and ν_{ck} are not independent, and likewise for μ_{sk} and ν_{sk}, it is convenient as before to express them in terms of a new set of variables:

$$
\begin{aligned}
\nu_{ck} &= N_{ck} + M_{ck},\ \mu_{ck} = M'_{ck} + N'_{c,k+1} \\
\nu_{sk} &= N_{sk} + M_{sk},\ \mu_{sk} = M'_{sk} + N'_{s,k+1}
\end{aligned}
\tag{10-106}
$$

where

$$N_{ck} = \int_{kT+\hat{\varepsilon}}^{(k+\frac{1}{2})T+\hat{\varepsilon}} n_c(t)dt,\ M_{ck} = \int_{(k+\frac{1}{2})T+\hat{\varepsilon}}^{(k+1)T+\hat{\varepsilon}} n_c(t)dt$$
$$N'_{ck} = \int_{kT+\hat{\varepsilon}}^{(k+\frac{\xi}{2})T+\hat{\varepsilon}} n_c(t)dt,\ M'_{ck} = \int_{(k+1-\frac{\xi}{2})T+\hat{\varepsilon}}^{(k+1)T+\hat{\varepsilon}} n_c\,(t)\,dt \tag{10-107}$$

with the properties

N_{ck}, M_{cn} are mutually independent for all k, n

N'_{ck}, M'_{cn} are mutually independent for all k, n

N'_{ck}, M_{cn} and M'_{ck}, N_{cn} are mutually independent for all k, n

N'_{ck}, N'_{cn} and M_{ck}, M_{cn} are mutually independent for all $k \neq n$

Furthermore, all $M_{ck}, M'_{ck}, N_{ck}, N'_{ck}$, and their sums are Gaussian random variables with zero mean and variances

$$\sigma^2_{M_{ck}} = \sigma^2_{N_{ck}} = N_0T/4$$
$$\sigma^2_{M'_{ck}} = \sigma^2_{N'_{ck}} = \xi N_0T/4 \tag{10-108}$$

Analogous definitions and properties apply to the sine channel noise variables.

Taking the difference of two successive soft decisions, X_{ck} and $X_{c,k+1}$ (or X_{sk} and $X_{s,k+1}$), and multiplying the average of the result by the quadrature I&D output, Y_{ck} (or Y_{sk}), delayed by $(1-\xi/2)\,T$ gives the sine and cosine channel error signal components in the kth symbol interval:

$$\begin{aligned} e_{ck} = {} & \left(b_k\cos\theta_c + \left(M'_{ck}+N'_{c,k+1}\right)\cos\theta_c - \left(M'_{sk}+N'_{s,k+1}\right)\sin\theta_c\right) \\ & \times\frac{1}{2}\left\{\left[c_k\cos\theta_c + (N_{ck}+M_{ck})\cos\theta_c - (N_{sk}+M_{sk})\sin\theta_c\right]\right. \\ & \left. -\ \left[c_{k+1}\cos\theta_c + (N_{c,k+1}+M_{c,k+1})\cos\theta_c - (N_{s,k+1}+M_{s,k+1})\sin\theta_c\right]\right\} \end{aligned} \tag{10-109}$$

and

$$
\begin{aligned}
e_{sk} = & \left(b_k \sin\theta_c + \left(M'_{ck} + N'_{c,k+1}\right)\sin\theta_c + \left(M'_{sk} + N'_{s,k+1}\right)\cos\theta_c\right) \\
& \times \frac{1}{2}\left\{\left[c_k \sin\theta_c + (N_{ck} + M_{ck})\sin\theta_c + (N_{sk} + M_{sk})\cos\theta_c\right]\right. \\
& \left. - \left[c_{k+1}\sin\theta_c + (N_{c,k+1} + M_{c,k+1})\sin\theta_c + (N_{s,k+1} + M_{s,k+1})\cos\theta_c\right]\right\}
\end{aligned} \tag{10-110}
$$

The total error signal, e_k, is the sum of the two components in Eqs. (10-110) and (10-109).

10.6.2.3 S-Curve Performance. The S-curve is by definition the statistical average of the error signal over the signal and noise probability distributions. Letting $\lambda \triangleq \varepsilon - \hat{\varepsilon}$ denote the normalized timing error ($-1/2 \le \lambda \le 1/2$), the S-curve $g(\lambda)$ becomes

$$
\begin{aligned}
g(\lambda) &= E_{n,s}\{e_{ck} + e_{sk}\} \\
&= E_s\left\{b_k\left(\frac{c_k - c_{k+1}}{2}\right)\cos^2\theta_c + b_k\left(\frac{c_k - c_{k+1}}{2}\right)\sin^2\theta_c\right\} \\
&= E_s\left\{b_k\left(\frac{c_k - c_{k+1}}{2}\right)\right\}
\end{aligned} \tag{10-111}
$$

which is independent of the carrier phase error as expected and also identical to the result for the coherent LDTTL. Thus, using the results from Section 4.1 with a slight simplification in the notation, i.e., ignoring the gain constants K_1 and K_2, we have

$$
g_n(\lambda) \triangleq \frac{g(\lambda)}{PT^2} = \begin{cases} \lambda\left(1 - \dfrac{\xi}{4}\right) - \dfrac{3}{2}\lambda^2, & 0 \le \lambda \le \dfrac{\xi}{2} \\ \dfrac{\xi}{2}(1 - 2\lambda), & \dfrac{\xi}{2} \le \lambda \le \dfrac{1}{2} \end{cases} \tag{10-112}
$$

As noted there, the normalized S-curve for the LDTTL is independent of SNR, whereas that for the conventional (nonlinear) DTTL is highly dependent on SNR. Taking the derivative of Eq. (10-112) with respect to λ and evaluating the result at $\lambda = 0$ gives the slope of the normalized S-curve at the origin, namely,

$$K_g \triangleq \frac{dg(\lambda)}{d\lambda}\,|_{\lambda=0} = PT^2\left(1-\frac{\xi}{4}\right) \tag{10-113}$$

10.6.2.4 Noise Performance. The equivalent noise $n_\lambda(t)$ perturbing the loop is characterized by the variation of the loop error signal around its mean (the S-curve) as in Eq. (10-27). Following the same approach as that taken in Section 10.3.2, then after some laborious analysis, we arrive at the equivalent noise power spectral density given by Eq. (10-30), where now

$$\begin{aligned} E_{n,s}\left\{e_n^2\,|_{\lambda=0}\right\} &= P^2T^4\left[\frac{\xi}{4R_s}\left(1+\frac{\xi}{2}+\frac{1}{R_s}\right)\right] \\ E_{n,s}\left\{e_n e_{n+m}\,|_{\lambda=0}\right\} &= \begin{cases} -P^2T^4\dfrac{\xi^2}{32R_s}, & m=1 \\ 0, & m>1 \end{cases} \end{aligned} \tag{10-114}$$

Substituting Eq. (10-114) into Eq. (10-30) gives the desired equivalent power spectral density as

$$N_0' = P^2T^5\frac{\xi}{2R_s}\left(1+\frac{\xi}{4}+\frac{1}{R_s}\right) \tag{10-115}$$

Interestingly enough, the result for the coherent LDTTL is given by [see Eq. (10-37)]

$$N_0' = P^2T^5\frac{\xi}{2R_s}\left(1+\frac{\xi}{4}+\frac{1}{2R_s}\right) \tag{10-116}$$

although by comparison the mathematics employed to arrive at Eq. (10-116) is considerably simpler than that needed to arrive at Eq. (10-115).

10.6.2.5 Mean-Squared Timing-Error Performance. The mean-squared timing error σ_λ^2 of the noncoherent LDTTL is readily computed for a first-order loop filter and large loop SNR conditions using the relation in Eq. (10-39), where now K_g is obtained from Eq. (10-113) and N_0' from Eq. (10-115). Making the appropriate substitutions in Eq. (10-39) gives the result

$$\sigma_\lambda^2\,|_{\text{NC-LDTTL}} = \frac{\xi\left(1+\dfrac{\xi}{4}+\dfrac{1}{R_s}\right)}{2\rho\left(1-\dfrac{\xi}{4}\right)^2} \tag{10-117}$$

which is to be compared with a similar result in Eq. (10-40) for the coherent LDTTL.

10.6.2.6 Tracking Performance of the Noncoherent Nonlinear DTTL. For the nonlinear noncoherent DTTL illustrated in Fig. 10-16, analogous to Eqs. (10-109) and (10-110), the error signal components are now given by

$$\begin{aligned} e_{ck} &= Y_{ck} \times \frac{1}{2}\left[\frac{X_{ck}}{\sqrt{X_{ck}^2+X_{sk}^2}} - \frac{X_{c,k+1}}{\sqrt{X_{c,k+1}^2+X_{s,k+1}^2}}\right] \\ &= \left(b_k\cos\theta_c + \left(M'_{ck}+N'_{c,k+1}\right)\cos\theta_c - \left(M'_{sk}+N'_{s,k+1}\right)\sin\theta_c\right) \\ &\quad\times\frac{1}{2}\left[\frac{(c_k+N_{ck}+M_{ck})\cos\theta_c-(N_{sk}+M_{sk})\sin\theta_c}{\sqrt{(c_k+N_{ck}+M_{ck})^2+(N_{sk}+M_{sk})^2}}\right. \\ &\quad\left.-\frac{(c_{k+1}+N_{c,k+1}+M_{c,k+1})\cos\theta_c-(N_{s,k+1}+M_{s,k+1})\sin\theta_c}{\sqrt{(c_{k+1}+N_{c,k+1}+M_{c,k+1})^2+(N_{s,k+1}+M_{s,k+1})^2}}\right] \end{aligned} \tag{10-118}$$

and

$$\begin{aligned} e_{sk} &= Y_{sk} \times \frac{1}{2}\left[\frac{X_{sk}}{\sqrt{X_{ck}^2+X_{sk}^2}} - \frac{X_{s,k+1}}{\sqrt{X_{c,k+1}^2+X_{s,k+1}^2}}\right] \\ &= \left(b_k\sin\theta_c + \left(M'_{ck}+N'_{c,k+1}\right)\sin\theta_c + \left(M'_{sk}+N'_{s,k+1}\right)\cos\theta_c\right) \\ &\quad\times\frac{1}{2}\left[\frac{(c_k+N_{ck}+M_{ck})\sin\theta_c+(N_{sk}+M_{sk})\cos\theta_c}{\sqrt{(c_k+N_{ck}+M_{ck})^2+(N_{sk}+M_{sk})^2}}\right. \\ &\quad\left.-\frac{(c_{k+1}+N_{c,k+1}+M_{c,k+1})\sin\theta_c+(N_{s,k+1}+M_{s,k+1})\cos\theta_c}{\sqrt{(c_{k+1}+N_{c,k+1}+M_{c,k+1})^2+(N_{s,k+1}+M_{s,k+1})^2}}\right] \end{aligned} \tag{10-119}$$

The total error signal, e_k, is now the sum of Eqs. (10-118) and (10-119), which after some trigonometric simplification becomes

$$e_k = \frac{1}{2}\left(b_k + M'_{ck} + N'_{c,k+1}\right)\left[\frac{c_k + N_{ck} + M_{ck}}{\sqrt{\left(c_k + N_{ck} + M_{ck}\right)^2 + \left(N_{sk} + M_{sk}\right)^2}}\right.$$

$$\left. - \frac{c_{k+1} + N_{c,k+1} + M_{c,k+1}}{\sqrt{\left(c_{k+1} + N_{c,k+1} + M_{c,k+1}\right)^2 + \left(N_{s,k+1} + M_{s,k+1}\right)^2}}\right]$$

$$+ \frac{1}{2}\left(M'_{sk} + N'_{s,k+1}\right)\left[\frac{N_{sk} + M_{sk}}{\sqrt{\left(c_k + N_{ck} + M_{ck}\right)^2 + \left(N_{sk} + M_{sk}\right)^2}}\right.$$

$$\left. - \frac{N_{s,k+1} + M_{s,k+1}}{\sqrt{\left(c_{k+1} + N_{c,k+1} + M_{c,k+1}\right)^2 + \left(N_{s,k+1} + M_{s,k+1}\right)^2}}\right] \qquad (10\text{-}120)$$

which is clearly independent of the unknown carrier phase, θ_c, as desired. To analytically compute even just the S-curve, much less the equivalent power spectral density, is now a daunting if not impossible task. Thus, in order to determine the tracking performance of this scheme, we shall have to turn to results obtained from computer simulations. Before doing this, however, we do note that in the absence of noise (i.e., in the limit of infinite SNR), the error signal of Eq. (10-120) becomes

$$e_k = b_k \frac{\operatorname{sgn} c_k - \operatorname{sgn} c_{k+1}}{2} \qquad (10\text{-}121)$$

which is the exact same result as for the coherent conventional (nonlinear) DTTL, and thus one can anticipate that, in the limit of large SNR, the noncoherent scheme should suffer little or no performance penalty relative to the coherent one. To demonstrate this as well as the behavior of the symbol synchronizer in other SNR regions, we turn to results obtained from computer simulation.

Figures 10-17 and 10-18 are illustrations of the normalized S-curves for the NC-NLDTTL for two different values of normalized window width and a variety of SNR values. The curves were obtained by numerically averaging the error signal of Eq. (10-120) over the data and noise statistics Also superimposed on

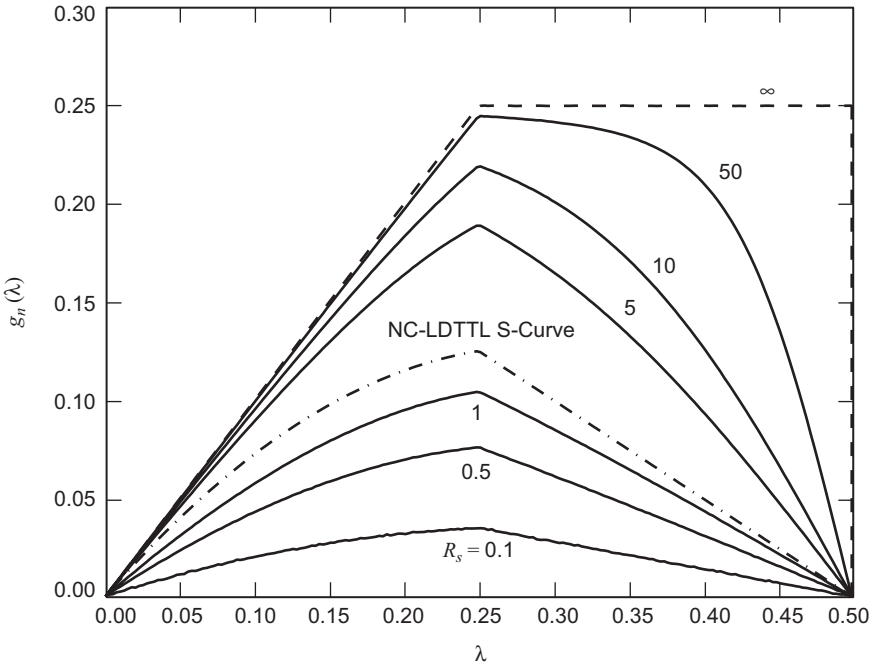

Fig. 10-17. NC-NLDTTL S-curve; $\xi = 0.5$.

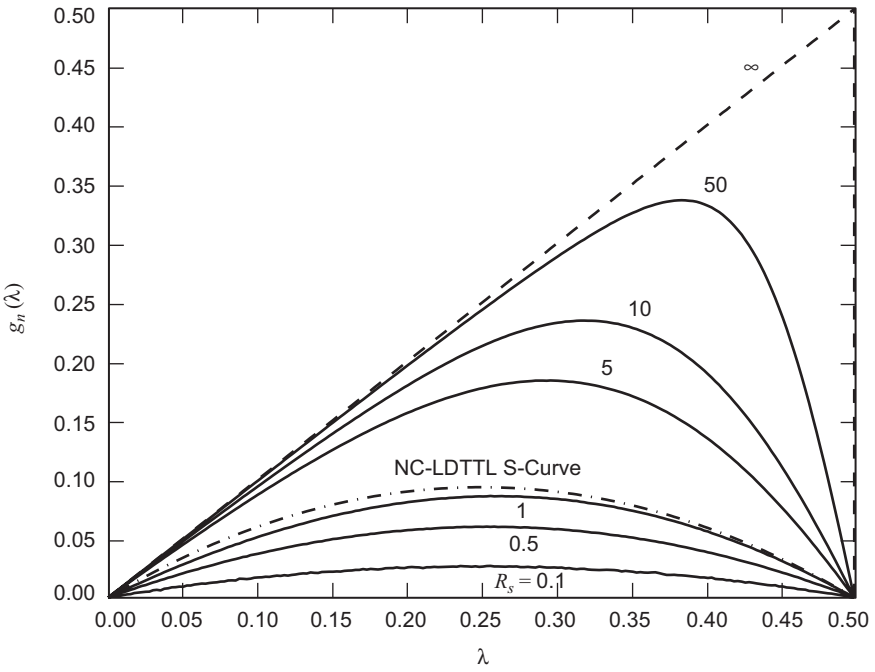

Fig. 10-18. NC-NLDTTL S-curve; $\xi = 1.0$.

these results are the corresponding S-curves for the NC-LDTTL as obtained from Eq. (10-112), which as previously mentioned are independent of SNR.

To demonstrate the performance trade-off of the noncoherent versus the coherent DTTL schemes as a function of SNR, Figs. 10-19 and 10-20 plot the mean-squared timing-error ratios $\sigma_\lambda^2\,|_{\text{NC-NLDTTL}}\,/\sigma_\lambda^2\,|_{\text{DTTL}}$ and $\sigma_\lambda^2\,|_{\text{NC-LDTTL}}\,/\sigma_\lambda^2\,|_{\text{LDTTL}}$, respectively, in dB versus SNR in dB for three different values of normalized window width ξ. For the first of the two ratios, the variance $\sigma_\lambda^2\,|_{\text{NC-NLDTTL}}$ is obtained by computer simulation and then divided by the variance of the conventional (nonlinear) DTTL obtained from the results in [1] as

$$\sigma_\lambda^2\,|_{\text{DTTL}} = \frac{\xi\left(1+\dfrac{\xi R_s}{2}-\dfrac{\xi}{2}\left[\dfrac{1}{\sqrt{\pi}}\exp\left(-R_s\right)+\sqrt{R_s}\,\text{erf}\sqrt{R_s}\right]^2\right)}{2\rho\left(\text{erf}\sqrt{R_s}-\dfrac{\xi}{2}\sqrt{\dfrac{R_s}{\pi}}\exp\left(-R_s\right)\right)^2} \tag{10-122}$$

The second of the two ratios is simply obtained from the division of Eq. (10-117) by Eq. (10-40). In both cases we observe that, as expected, the noncoherent and coherent performances approach each other as the SNR gets large (i.e., the above variance ratios approach unity or 0 dB). In the limit of infinitesimally small SNR, the noncoherent schemes pay a performance penalty with respect to the coherent schemes, which in the linear case is easily computed from Eqs. (10-117) and (10-40) to be 3 dB, while in the nonlinear case it appears to be somewhat less and mildly dependent on the window width. Finally, a comparison between the noncoherent linear and nonlinear DTTL performances is illustrated in Fig. 10-21, where the ratio of $\sigma_\lambda^2\,|_{\text{NC-LDTTL}}$ to $\sigma_\lambda^2\,|_{\text{NC-NLDTTL}}$ in dB is plotted versus SNR, R_s, in dB for a variety of different window widths. Analogous to a similar plot for the coherent DTTL schemes in Fig. 10-6, for each window width there exists a crossover point at which the variance ratio equals unity (or, equivalently, 0 dB), indicating the value of SNR that separates the SNR regions where one scheme is preferable over the other.

10.7 The Impact of Carrier Frequency Offset on Performance

Thus far in our discussions of noncoherent symbol synchronization, the word "noncoherent" was used to mean that the carrier phase was completely unknown [i.e., uniformly distributed in the interval $(-\pi, \pi)$] but at the same time the carrier frequency was assumed to be known exactly. Here, as an example,

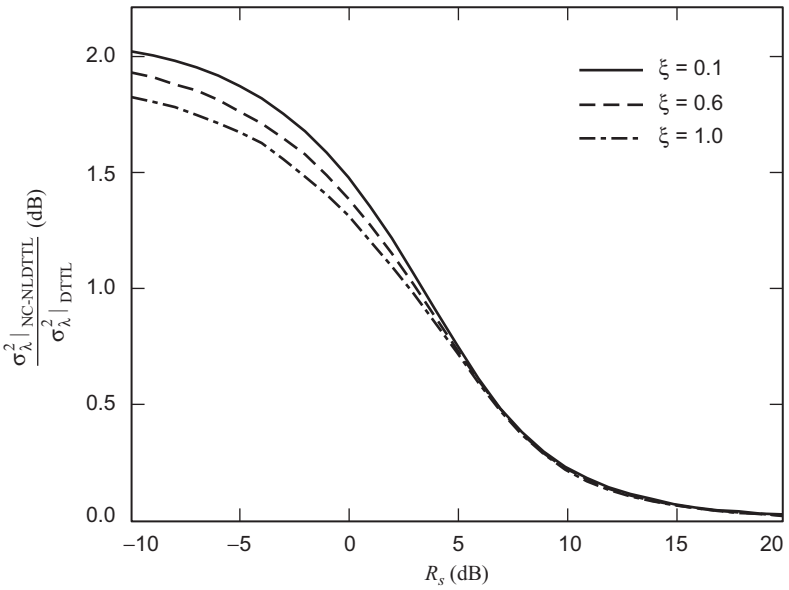

Fig. 10-19. The ratio of the mean-squared timing error for the noncoherent nonlinear DTTL to that of the coherent nonlinear DTTL with window width (ξ) as a parameter.

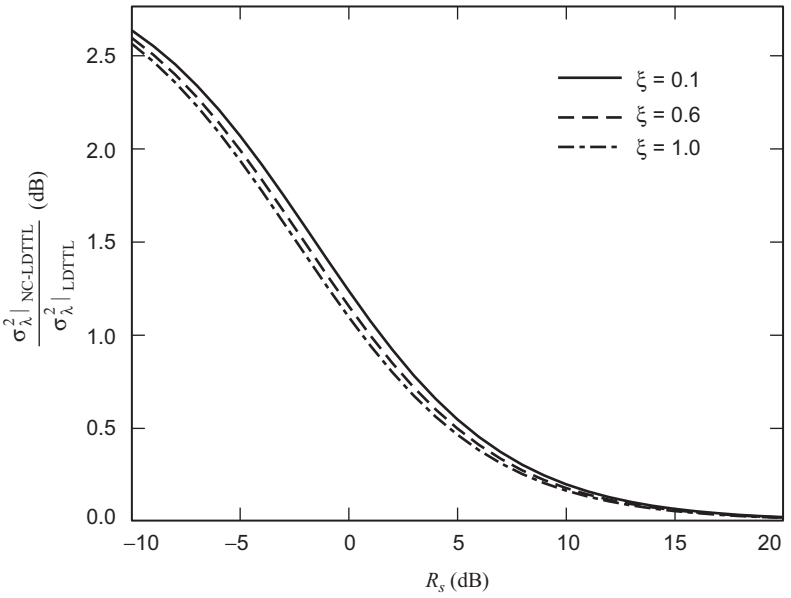

Fig. 10-20. The ratio of the mean-squared timing error for the noncoherent linear DTTL to that of the coherent linear DTTL with window width (ξ) as a parameter.

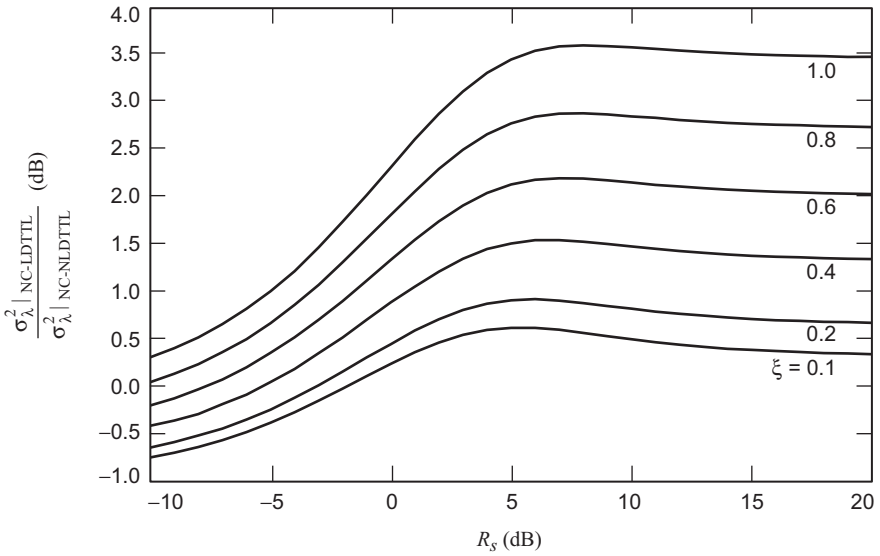

Fig. 10-21. The ratio of the mean-squared timing error for the noncoherent linear DTTL to that of the noncoherent nonlinear DTTL with window width (ξ) as a parameter.

we investigate the impact on the performance of the NC-LDTTL of imperfect knowledge of the carrier frequency, i.e., the presence of a fixed carrier frequency offset. In particular, we shall briefly rederive the expression for the variance of the normalized timing error in the loop and demonstrate its exact dependence on the ratio of symbol rate to frequency offset. Comparing this expression with that corresponding to the zero frequency offset case allows us to assess the additional degradation in performance that arises from the presence of the offset.

Consider the NC-LDTTL illustrated in Fig. 10-15, whose bandpass input $r(t) = s(t,\varepsilon) + n(t)$ is as before a BPSK modulation consisting of a binary NRZ data stream direct-modulated onto a carrier plus noise. While the signal component $s(t,\varepsilon)$ of this input will still be modeled as in the combination of Eq. (10-65) with Eq. (10-64), as we shall discuss momentarily it will be mathematically convenient to choose a slightly different representation of the bandpass noise $n(t)$ than the one given in Eq. (10-65).

The first step is to demodulate the received signal with the quadrature carrier reference signals

$$\begin{aligned} r_c(t) &= \sqrt{2}\cos\hat{\omega}_c t \\ r_s(t) &= -\sqrt{2}\sin\hat{\omega}_c t \end{aligned} \tag{10-123}$$

whose frequency is now assumed to be in error by an amount $\Delta\omega = \omega_c - \hat{\omega}_c$. Since the choice of frequency and phase used for representation of a bandpass noise process is arbitrary, for the purpose of analysis we choose these parameters corresponding to those of the carrier demodulation reference signals, in which case we have

$$n(t) = \sqrt{2}\left[n_c(t)\cos\hat{\omega}_c t - n_s(t)\sin\hat{\omega}_c t\right] \tag{10-124}$$

where $n_c(t), n_s(t)$ are as before low-pass AWGN processes with two-sided power spectral density (PSD) $N_0/2$ W/Hz. Thus, demodulating $r(t)$ with the quadrature reference signals of Eq. (10-123) results in the pair of baseband observables in the kth symbol interval $(k+\varepsilon)T \le t \le (k+1+\varepsilon)T$,

$$\begin{aligned} x_{ck}(t) &= \sqrt{P}d_k p\big(t-(k+\varepsilon)T\big)\cos\left(\Delta\omega t + \theta_c\right) + n_c(t) \\ x_{sk}(t) &= \sqrt{P}d_k p\big(t-(k+\varepsilon)T\big)\sin\left(\Delta\omega t + \theta_c\right) + n_s(t) \end{aligned} \tag{10-125}$$

Analogous to Eq. (10-104), the outputs of the I and Q I&D filters are now

$$\begin{aligned} X_{ck} &= \int_{kT+\hat{\varepsilon}}^{(k+1)T+\hat{\varepsilon}} x_{ck}(t)dt \\ &= \overbrace{\int_{kT+\hat{\varepsilon}}^{(k+1)T+\hat{\varepsilon}} \sqrt{P}d_k\cos\left(\Delta\omega t+\theta_c\right)dt}^{c_{ck}} + \overbrace{\int_{kT+\hat{\varepsilon}}^{(k+1)T+\hat{\varepsilon}} n_c(t)\,dt}^{\nu_{ck}} \\ Y_{ck} &= \int_{\left(k+1-\frac{\xi}{2}\right)T+\hat{\varepsilon}}^{\left(k+1+\frac{\xi}{2}\right)T+\hat{\varepsilon}} x_{ck}(t)dt \\ &= \overbrace{\int_{\left(k+1-\frac{\xi}{2}\right)T+\hat{\varepsilon}}^{\left(k+1+\frac{\xi}{2}\right)T+\hat{\varepsilon}} \sqrt{P}d_k\cos\left(\Delta\omega t+\theta_c\right)dt}^{b_{ck}} + \overbrace{\int_{\left(k+1-\frac{\xi}{2}\right)T+\hat{\varepsilon}}^{\left(k+1+\frac{\xi}{2}\right)T+\hat{\varepsilon}} n_c(t)\,dt}^{\mu_{ck}} \end{aligned} \tag{10-126}$$

and

$$
\begin{aligned}
X_{sk} &= \int_{kT+\hat{\varepsilon}}^{(k+1)T+\hat{\varepsilon}} x_{sk}(t)dt \\
&= \overbrace{\int_{kT+\hat{\varepsilon}}^{(k+1)T+\hat{\varepsilon}} \sqrt{P} d_k \sin\left(\Delta\omega t + \theta_c\right) dt}^{c_{sk}} + \overbrace{\int_{kT+\hat{\varepsilon}}^{(k+1)T+\hat{\varepsilon}} n_s\left(t\right) dt}^{\nu_{sk}} \\
Y_{sk} &= \int_{\left(k+1-\frac{\xi}{2}\right)T+\hat{\varepsilon}}^{\left(k+1+\frac{\xi}{2}\right)T+\hat{\varepsilon}} x_{sk}(t)dt \\
&= \overbrace{\int_{\left(k+1-\frac{\xi}{2}\right)T+\hat{\varepsilon}}^{\left(k+1+\frac{\xi}{2}\right)T+\hat{\varepsilon}} \sqrt{P} d_k \sin(\Delta\omega t + \theta_c) dt}^{b_{sk}} + \overbrace{\int_{\left(k+1-\frac{\xi}{2}\right)T+\hat{\varepsilon}}^{\left(k+1+\frac{\xi}{2}\right)T+\hat{\varepsilon}} n_s\left(t\right) dt}^{\mu_{sk}}
\end{aligned}
\tag{10-127}
$$

Taking the difference of two successive soft decisions, X_{ck} and $X_{c,k+1}$ (or X_{sk} and $X_{s,k+1}$), and multiplying the average of the result by the quadrature I&D output Y_{ck} (or Y_{sk}), delayed by $(1-\xi/2)\,T$, gives the sine and cosine channel error signal components in the kth symbol interval:

$$
e_{ck} = \left(b_{ck} + M'_{ck} + N'_{c,k+1}\right) \frac{\left(c_{ck} + N_{ck} + M_{ck}\right) - \left(c_{c,k+1} + N_{c,k+1} + M_{c,k+1}\right)}{2}
\tag{10-128}
$$

and

$$
e_{sk} = \left(b_{sk} + M'_{sk} + N'_{s,k+1}\right) \frac{\left(c_{ck} + N_{sk} + M_{sk}\right) - \left(c_{s,k+1} + N_{s,k+1} + M_{s,k+1}\right)}{2}
\tag{10-129}
$$

The total error signal, e_k, is again the sum of the two components in Eqs. (10-128) and (10-129).

10.7.1 S-Curve Performance

Using Eqs. (10-128) and (10-129), the S-curve $g\left(\lambda\right)$ is evaluated as

$$
\begin{aligned}
g(\lambda) &= E_{n,s}\left\{e_{ck} + e_{sk}\right\} \\
&= E_s\left\{b_{ck}\left(\frac{c_{ck} - c_{c,k+1}}{2}\right) + b_{sk}\left(\frac{c_{sk} - c_{s,k+1}}{2}\right)\right\}
\end{aligned}
\tag{10-130}
$$

which as we shall see shortly is still independent of the carrier phase but is now dependent on the frequency offset. Evaluating the signal terms in Eq. (10-130), whose definition appears in Eqs. (10-126) and (10-127), and carrying out the necessary integrations, we arrive at the following results:

$$\begin{aligned} c_{ck} =& \sqrt{P} d_{k-1} \lambda T \left(\frac{\sin \pi \eta \lambda}{\pi \eta \lambda} \right) \cos \left(2\pi \eta \left(k + \frac{\lambda}{2} \right) + \theta \right) \\ &+ \sqrt{P} d_k \lambda T \left(\frac{\sin \pi \eta (1-\lambda)}{\pi \eta (1-\lambda)} \right) \cos \left(2\pi \eta \left(k + \frac{1}{2} + \frac{\lambda}{2} \right) + \theta \right) \end{aligned} \tag{10-131}$$

$$\begin{aligned} b_{ck} =& \sqrt{P} d_k \left(\frac{\xi}{2} + \lambda \right) T \left(\frac{\sin \pi \eta \left(\frac{\xi}{2} + \lambda \right)}{\pi \eta \left(\frac{\xi}{2} + \lambda \right)} \right) \cos \left(2\pi \eta \left(k + 1 + \frac{\lambda - \frac{\xi}{2}}{2} \right) + \theta \right) \\ &+ \sqrt{P} d_{k+1} \left(\frac{\xi}{2} - \lambda \right) T \left(\frac{\sin \eta \left(\frac{\xi}{2} - \lambda \right)}{\eta \left(\frac{\xi}{2} - \lambda \right)} \right) \cos \left(2\pi \eta \left(k + 1 + \frac{\lambda + \frac{\xi}{2}}{2} \right) + \theta \right) \end{aligned}$$

and

$$\begin{aligned} c_{sk} =& -\sqrt{P} d_{k-1} \lambda T \left(\frac{\sin \pi \eta \lambda}{\pi \eta \lambda} \right) \sin \left(2\pi \eta \left(k + \frac{\lambda}{2} \right) + \theta \right) \\ &- \sqrt{P} d_k \lambda T \left(\frac{\sin \pi \eta (1-\lambda)}{\pi \eta (1-\lambda)} \right) \sin \left(2\eta \left(k + \frac{1}{2} + \frac{\lambda}{2} \right) + \theta \right) \end{aligned} \tag{10-132}$$

$$\begin{aligned} b_{sk} =& -\sqrt{P} d_k \left(\frac{\xi}{2} + \lambda \right) T \left(\frac{\sin \pi \eta \left(\frac{\xi}{2} + \lambda \right)}{\pi \eta \left(\frac{\xi}{2} + \lambda \right)} \right) \sin \left(2\pi \eta \left(k + 1 + \frac{\lambda - \frac{\xi}{2}}{2} \right) + \theta \right) \\ &- \sqrt{P} d_{k+1} \left(\frac{\xi}{2} - \lambda \right) T \left(\frac{\sin \pi \eta \left(\frac{\xi}{2} - \lambda \right)}{\pi \eta \left(\frac{\xi}{2} - \lambda \right)} \right) \sin \left(2\pi \eta \left(k + 1 + \frac{\lambda + \frac{\xi}{2}}{2} \right) + \theta \right) \end{aligned}$$

where $\eta \triangleq \Delta\omega T/2\pi = \Delta f T$. Finally, substituting Eqs. (10-131) and (10-132) into Eq. (10-130) and performing the average over the data symbols gives, after some trigonometric simplification,[15]

$$
\begin{aligned}
g_n(\lambda) \triangleq & \frac{g(\lambda)}{PT^2} \\
= & \frac{1}{2}(1-\lambda)\left(\frac{\xi}{2}+\lambda\right)\left(\frac{\sin\pi\eta(1-\lambda)}{\pi\eta(1-\lambda)}\right)\left(\frac{\sin\pi\eta\left(\frac{\xi}{2}+\lambda\right)}{\pi\eta\left(\frac{\xi}{2}+\lambda\right)}\right)\cos\pi\eta\left(1-\frac{\xi}{2}\right) \\
& -\frac{1}{2}\lambda\left(\frac{\xi}{2}+\lambda\right)\left(\frac{\sin\pi\eta\lambda}{\pi\eta\lambda}\right)\left(\frac{\sin\pi\eta\left(\frac{\xi}{2}+\lambda\right)}{\pi\eta\left(\frac{\xi}{2}+\lambda\right)}\right)\cos\pi\eta\frac{\xi}{2} \\
& -\frac{1}{2}(1-\lambda)\left(\frac{\xi}{2}-\lambda\right)\left(\frac{\sin\pi\eta(1-\lambda)}{\pi\eta(1-\lambda)}\right)\left(\frac{\sin\pi\eta\left(\frac{\xi}{2}-\lambda\right)}{\pi\eta\left(\frac{\xi}{2}-\lambda\right)}\right)\cos\pi\eta\left(1-\frac{\xi}{2}\right); \\
& \qquad 0 \le \lambda \le \frac{\xi}{2}
\end{aligned}
\tag{10-133}
$$

In the case of no frequency offset ($\eta = 0$), the S-curve of Eq. (10-133) simplifies to Eq. (10-112) as it should.

Taking the derivative of Eq. (10-133) with respect to λ and evaluating the result at $\lambda = 0$ gives the slope of the S-curve at the origin as

$$
\begin{aligned}
K_g \triangleq \frac{dg(\lambda)}{d\lambda}\Big|_{\lambda=0} &= PT^2\left\{\left(\frac{\sin\pi\eta\xi/2}{\pi\eta\xi/2}\right)\right. \\
&\left.\times\left[1+\left(\frac{\sin\pi\eta}{\pi\eta}\right)\cos\pi\eta(1-\xi/2)-\frac{\xi}{4}\cos\pi\eta\xi/2\right]-\cos\pi\eta\xi/2\right\}
\end{aligned}
\tag{10-134}
$$

which in the case of no frequency offset ($\eta = 0$) simplifies to Eq. (10-113).

---

[15] For the sake of brevity, we do not present the result for the S-curve in the region $\xi/2 \le \lambda \le 1/2$ since for the purpose of mean-squared timing-error evaluation we have already seen that only the slope of the S-curve at the origin ($\lambda = 0$) is needed.

10.7.2 Noise Performance

As before, we must determine the PSD at $\lambda = 0$ of the equivalent noise, $n_\lambda(t)$, perturbing the loop as given by Eq. (10-30). Following an analogous approach to that taken for the zero frequency offset case, the following results are obtained:

$$E_{n,s}\left\{e_k^2\,|_{\lambda=0}\right\} = P^2T^4\left(\frac{\xi}{4R_s}\right)\left[\left(\frac{\sin\pi\eta}{\pi\eta}\right)^2 + \frac{\xi}{2}\left(\frac{\sin\pi\eta\xi/2}{\pi\eta\xi/2}\right)^2 + \frac{1}{R_s}\right] \tag{10-135}$$

$$E_{n,s}\left\{e_k e_{k+1}\,|_{\lambda=0}\right\} = \begin{cases} -P^2T^4\left(\dfrac{\xi^2}{32R_s}\right)\cos 2\pi\eta\,(1-\xi/2)\,, & m=1 \\ 0, & m>1 \end{cases}$$

where as before $R_s \triangleq PT/N_0$ denotes the detection symbol SNR. Substituting Eq. (10-135) into Eq. (10-30) gives the desired equivalent PSD as

$$N_0' = P^2T^5\left(\frac{\xi}{2R_s}\right)\left\{\left(\frac{\sin\pi\eta}{\pi\eta}\right)^2 + \frac{\xi}{2}\left[\left(\frac{\sin\pi\eta\xi/2}{\pi\eta\xi/2}\right)^2 - \frac{1}{2}\cos 2\pi\eta\,(1-\xi/2)\right] + \frac{1}{R_s}\right\} \tag{10-136}$$

10.7.3 Mean-Squared Timing-Error Performance

The mean-squared timing error σ_λ^2 of the LDTTL in the presence of frequency offset is now readily computed using the results in Eqs. (10-134) and (10-136) in Eq. (10-39), resulting in

$$\sigma_\lambda^2 = \frac{\xi\left\{\left(\dfrac{\sin\pi\eta}{\pi\eta}\right)^2 + \dfrac{\xi}{2}\left[\left(\dfrac{\sin\pi\eta\frac{\xi}{2}}{\pi\eta\frac{\xi}{2}}\right)^2 - \dfrac{1}{2}\cos 2\pi\eta\left(1-\dfrac{\xi}{2}\right)\right] + \dfrac{1}{R_s}\right\}}{2\rho\left\{\left(\dfrac{\sin\pi\eta\frac{\xi}{2}}{\pi\eta\frac{\xi}{2}}\right)\left[1 + \left(\dfrac{\sin\pi\eta}{\pi\eta}\right)\cos\pi\eta\left(1-\dfrac{\xi}{2}\right) - \dfrac{\xi}{4}\cos\pi\eta\dfrac{\xi}{2}\right] - \cos\pi\eta\dfrac{\xi}{2}\right\}^2} \tag{10-137}$$

For zero frequency offset ($\eta = 0$), Eq. (10-137) simplifies to Eq. (10-117).

To demonstrate the additional degradation in performance of the NC-LDTTL due to frequency offset, Fig. 10-22 plots the mean-squared timing-error ratio $\sigma_\lambda^2/\sigma_\lambda^2|_{\Delta f=0}$ in dB versus SNR in dB for several different values of normalized frequency offset, $\eta = \Delta fT$, and two different values of normalized window width, ξ. We observe from these results that over a wide range of SNRs the degradation is virtually insensitive to this parameter. Furthermore, the degradation also appears to be relatively insensitive to window width. Finally, for values of normalized frequency offset less than 0.1, it can be observed that the performance degradation is quite small (i.e., less than 0.5 dB).

10.7.4 A Final Note

Thus far in our discussion of the noncoherent DTTL in this section we have assumed an input signal in the form of BPSK modulation. Before concluding this section, we wish to point out that it is possible to apply the same MAP estimation approach to QPSK to arrive at LFs that can be used to motivate closed-loop symbol synchronizers for this modulation. Without going into detail, it can be shown that, under the same approximations used to derive the low and high SNR versions of the noncoherent DTTLs for BPSK, the LFs that result from this approach when applied to QPSK are identical to those obtained for BPSK. Equivalently stated, noncoherent symbol synchronization of QPSK with a DTTL type of structure takes on the exact same form as that for BPSK.

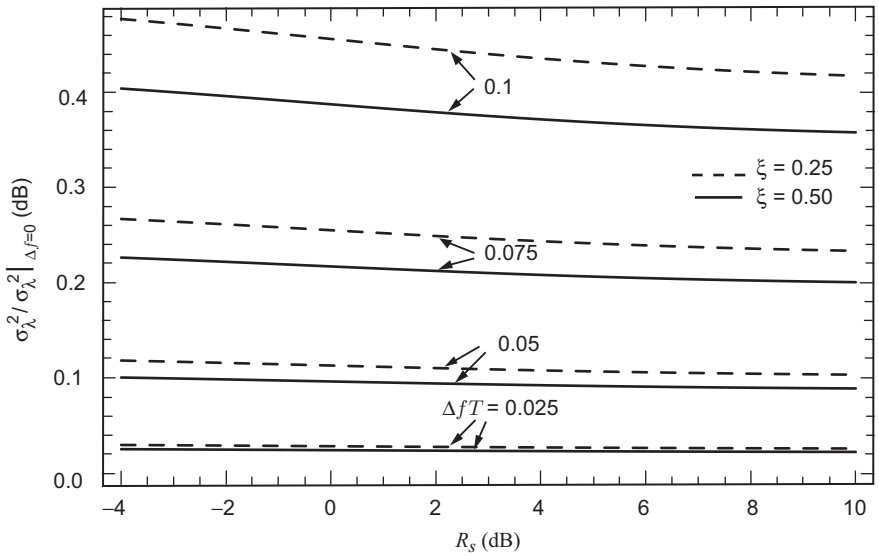

Fig. 10-22. Mean-squared timing-error performance degradation versus detection SNR with normalized frequency error as a parameter.

10.8 Coarse Estimation of Symbol Timing for Use in SNR Estimation

In our discussions of SNR estimation for autonomous receiver operation in Chapter 6, we considered the behavior of the split-symbol moments estimator (SSME) in the presence of unknown symbol timing. Although originally derived on the basis of perfect symbol sync information, it was shown there that, in the presence of unknown symbol timing, the performance of a conventional SSME becomes quite sensitive to the amount of symbol-timing error. In fact, in order to properly operate at all, the form of the estimator now requires knowledge (an estimate) of the symbol timing [via the parameters $\hat{h}^+$ and $\hat{h}^-$ in Eq. (6-54)]. Thus, it is essential that one provide a coarse estimate of symbol timing to the SNR estimator,[16] preferably derived from the same statistics as those used to form this estimator itself.

Using the relations for the mean of the sums U^+ and U^- of the squared magnitudes of the sum and difference half-symbol I&D outputs [see Eqs. (6-49) and (6-51)], we have

$$E\left\{U^+\right\} - E\left\{U^-\right\} = 2\sigma^2\left(\overline{h}^+ - \overline{h}^-\right)R = 2\sigma^2\left(1 - 2\left|\varepsilon\right|\right)R \tag{10-138}$$

While Eq. (10-138) provides the needed measure of the symbol timing, it also depends on σ^2 and R, which are parameters that themselves need to be estimated. Thus, it behooves us to find another measure of the product of σ^2 and R that is independent of the symbol sync timing, which could then be used together with Eq. (10-138) to isolate the $1 - 2\left|\varepsilon\right|$ factor.

Also considered in Chapter 6 was a modification of the conventional SSME that produced a set of observables obtained from oversampling the symbol interval by a factor L and as such was capable of providing improved performance at SNRs above 3 dB. It was also shown there that this same modification had the added advantage of reducing the sensitivity of the estimator performance to incorrect symbol-timing information and, in the limit of sufficiently large L, became completely insensitive to knowledge of ε. In fact, for L approaching infinity, the difference of the means considered in Eq. (10-138) now became [see Eq. (6-110)]

$$E\left\{U^+\right\} - E\left\{U^-\right\} = 2\sigma^2 R \tag{10-139}$$

[16] Actually, because of the noncoherent nature of the SNR estimator, it requires only an estimate of the *magnitude* of the symbol sync timing.

Hence, taking the ratio of Eq. (10-138) to Eq. (10-139) gives

$$\frac{\left(E\left\{U^{+}\right\}-E\left\{U^{-}\right\}\right)|_{L=1}}{\left(E\left\{U^{+}\right\}-E\left\{U^{-}\right\}\right)|_{L=\infty}}=1-2\left|\varepsilon\right| \tag{10-140}$$

which is the desired result. Thus, it follows from Eq. (10-140) that a coarse estimator of symbol timing based on the same statistics used to produce the SNR estimator is given by

$$\left|\hat{\varepsilon}\right|=\frac{1}{2}\left[1-\frac{\left(U^{+}-U^{-}\right)|_{L=1}}{\left(U^{+}-U^{-}\right)|_{L=\infty}}\right] \tag{10-141}$$

Since in practice one deals with a finite oversampling factor, what follows next is a quantification of the difference of means $E\left\{U^{+}\right\}-E\left\{U^{-}\right\}$ as a function of L to enable one to determine how large one must make L in order to reach the limiting value as in Eq. (10-139).

For a given oversampling factor L, we can characterize the fractional (with respect to T) symbol timing by $\varepsilon=\left(l_{\varepsilon}+1/2+\delta\right)/L,\ l_{\varepsilon}=0,1,2,\cdots,L-1$, where l_{ε} represents the integer number of symbol interval subdivisions and $|\delta|\leq 1/2$ represents the remaining fraction of a subdivision. Then, it is straightforward to see that for $L-1$ subdivisions both the entire first and second half-symbol I&Ds correspond to the same symbol, and thus the contribution of each of these subdivisions to the mean-squared accumulations U^{+} and U^{-} *is independent of* ε! More explicitly, for $l=1,2,\cdots,L-l_{\varepsilon}-1$, assuming for simplicity no frequency uncertainty, the first and second half-symbol I&D outputs are given by (see Section 6.11 for a description of the notation)

$$\begin{aligned}Y_{\alpha kl}&=\frac{md_{k}}{2}e^{j\phi}+n_{\alpha kl}\\ Y_{\beta kl}&=\frac{md_{k}}{2}e^{j\phi}+n_{\beta kl}\end{aligned} \tag{10-142}$$

and similarly for $l=L-l_{\varepsilon}+1,L-l_{\varepsilon}+2,\cdots,L$,

$$\begin{aligned}Y_{\alpha kl}&=\frac{md_{k+1}}{2}e^{j\phi}+n_{\alpha kl}\\ Y_{\beta kl}&=\frac{md_{k+1}}{2}e^{j\phi}+n_{\beta kl}\end{aligned} \tag{10-143}$$

where $n_{\alpha kl}$ and $n_{\beta kl}$ are complex Gaussian zero-mean noise variables with variance $\sigma^2 L$. This leaves one subdivision, i.e., the one corresponding to $l = L - l_\varepsilon$, to be affected by the lack of symbol sync knowledge. For this one subdivision, the first and second half-symbol I&D outputs are given by

$$\begin{aligned} Y_{\alpha kl}\,|_{l=L-l_\varepsilon} &= \frac{m}{2}\left[d_k\left(\frac{1}{2}-\delta\right)+d_{k+1}\delta\right]e^{j\phi}+n_{\alpha kl}\,|_{l=L-l_\varepsilon}, \\ Y_{\beta kl} &= \frac{md_{k+1}}{2}e^{j\phi}+n_{\beta kl}; \quad 0\le\delta\le\frac{1}{2} \\ Y_{\alpha kl}\,|_{l=L-l_\varepsilon} &= \frac{md_k}{2}e^{j\phi}+n_{\alpha kl}\,|_{l=L-l_\varepsilon}, \\ Y_{\beta kl} &= \frac{m}{2}\left[d_k\,|\delta|+d_{k+1}\left(\frac{1}{2}-|\delta|\right)\right]e^{j\phi}+n_{\beta kl}; \quad -\frac{1}{2}\le\delta\le 0 \end{aligned} \tag{10-144}$$

Forming the sum and difference signals from Eqs. (10-142) through (10-144), we get

$$\begin{aligned} u_{kl}^{+} &= md_k e^{j\phi}+n_{\alpha kl}+n_{\beta kl} \\ u_{kl}^{-} &= n_{\alpha kl}+n_{\beta kl}, \quad l=1,2,\cdots,L-l_\varepsilon-1 \\ u_{kl}^{+} &= md_{k+1}e^{j\phi}+n_{\alpha kl}+n_{\beta kl} \\ u_{kl}^{-} &= n_{\alpha kl}+n_{\beta kl}, \quad l=L-l_\varepsilon+1,L-l_\varepsilon+2,\cdots,L \\ u_{kl}^{\pm} &= m\left[d_k\left(\frac{1}{2}-\delta\right)+d_{k+1}\left(\delta\pm\frac{1}{2}\right)\right]e^{j\phi}+n_{\alpha kl}\pm n_{\beta kl}, \\ &\qquad 0\le\delta\le\frac{1}{2}, \quad l=L-l_\varepsilon \\ u_{kl}^{\pm} &= m\left[d_k\left(\frac{1}{2}\pm|\delta|\right)\pm d_{k+1}\left(|\delta|-\frac{1}{2}\right)\right]e^{j\phi}+n_{\alpha kl}\pm n_{\beta kl}, \\ &\qquad -\frac{1}{2}\le\delta\le 0, \quad l=L-l_\varepsilon \end{aligned} \tag{10-145}$$

Finally, the means of $U^{\pm}=(1/NL)\sum_{k=1}^{N}\sum_{l=1}^{L}\left|u_{kl}^{\pm}\right|^2$ are easily shown to be

$$E\left\{U^+\right\} = 2\sigma^2\left[L + R\left(1 - \frac{\frac{1}{2} - 2|\delta|^2}{L}\right)\right]$$
$$E\left\{U^-\right\} = 2\sigma^2\left[L + R\left(\frac{\frac{1}{2} - 2|\delta| + 2|\delta|^2}{L}\right)\right], \quad 0 \le |\delta| \le \frac{1}{2} \tag{10-146}$$

which agrees with the results in Eq. (6-110) when $|\delta| = 1/2$, i.e., a fractional (with respect to a subdivision of T) timing error equal to $1/2$.

References

[1] M. K. Simon, "An Analysis of the Steady-State Phase Noise Performance of a Digital Data-Transition Tracking Loop," *ICC '69 Conference Record*, Boulder, Colorado, pp. 20-9–20-15, June 1969. Also see M. K. Simon, *An Analysis of the Steady-State Phase Noise Performance of a Digital Data-Transition Tracking Loop*, JPL Technical Report 900-222, Jet Propulsion Laboratory, Pasadena, California, November 21, 1968.

[2] W. C. Lindsey and M. K. Simon, *Telecommunication Systems Engineering*, Englewood Cliffs, New Jersey: Prentice-Hall, 1973. Reprinted by Dover Press, New York, 1991.

[3] H. Cramer, *Mathematical Methods of Statistics*, Princeton, New Jersey: Princeton University, 1951.

[4] C. Rao, *Linear Statistical Inference and Its Application*, New York: John Wiley & Sons, 1965.

[5] H. V. Trees, *Detection, Estimation, and Modulation Theory*, New York: John Wiley & Sons, 1968.

[6] J. Ziv and M. Zakai, "Some Lower Bounds on Signal Parameter Estimation," *IEEE Transactions on Information Theory*, vol. IT-15, pp. 386–391, May 1969.

[7] D. Chasan, M. Zakai, and J. Ziv, "Improved Lower Bounds on Signal Parameter Estimation," *IEEE Transactions on Information Theory*, vol. IT-21, pp. 90–93, January 1975.

[8] I. Ibragimov and R. Khas′minskii, "Parameter Estimation for a Discontinuous Signal in White Gaussian Noise," *Problemy Peredachi Informatsii*, vol. 11, pp. 31–43, July–September 1975, as translated in *Problems of Information Transmission*, pp. 203–212, September 1976.

[9] A. Terent′yev, "Distribution of the Time of Absolute Maximum at the Output of a Matched Filter," *Radio Engineering and Electronic Physics*, vol. 13, no. 4, pp. 569–573, 1968.

[10] K. Kosbar, *Open and Closed Loop Delay Estimation with Applications to Pseudonoise Code Tracking*, Ph.D. thesis, University of Southern California, Los Angeles, California, July 1988.

[11] J. Holmes, "Tracking Performance of the Filter and Square Bit Synchronizer," *IEEE Transactions on Communications*, vol. COM-28, pp. 1154–1158, August 1980.

[12] R. D. McCallister and M. K. Simon, "Cross-Spectrum Symbol Synchronizer," *ICC'81 Conference Record*, pp. 34.3.1–34.3.6, 1981.

[13] S. Haykin, *Communication Systems*, New York: John Wiley & Sons, 4th ed., 2001.